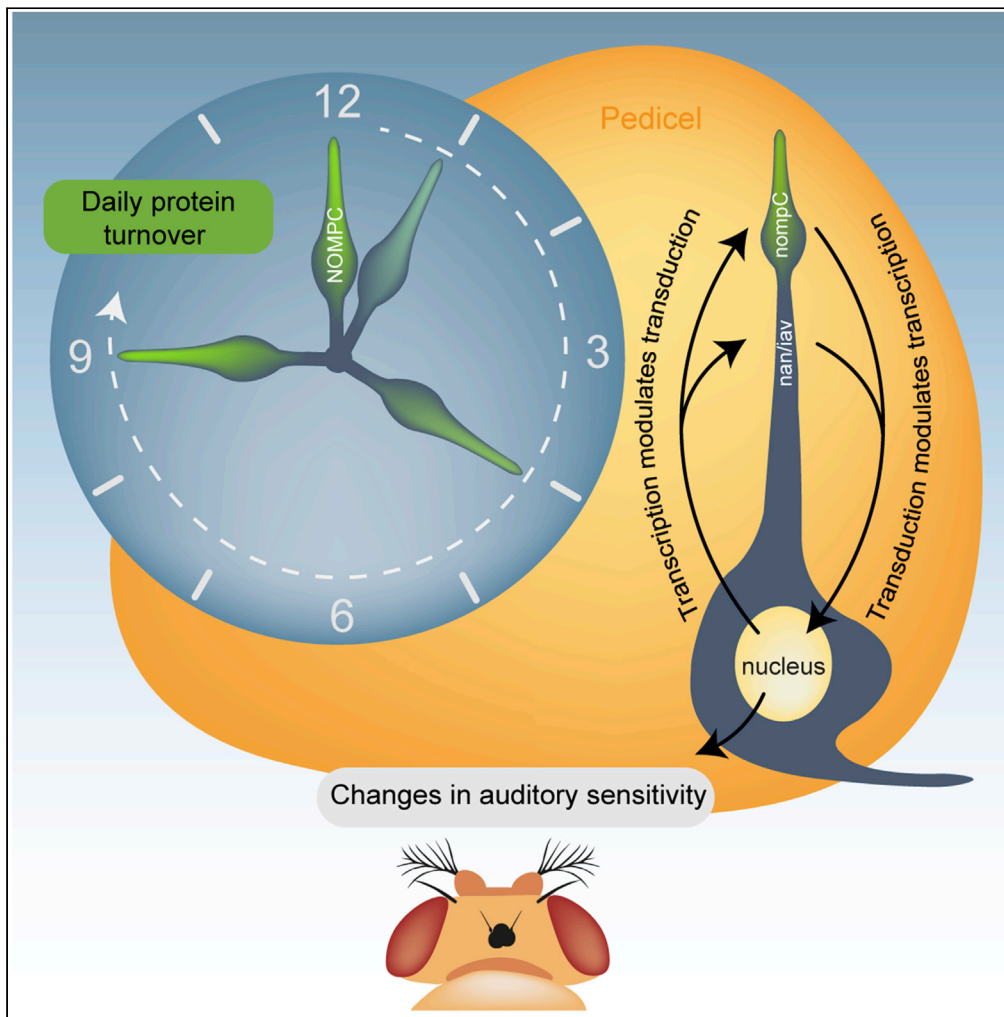


Article

Turnover and activity-dependent transcriptional control of NompC in the *Drosophila* ear



Nicholas Boyd-Gibbins, Camille H. Tardieu, Modesta Blunskyte, Nerissa Kirkwood, Jason Somers, Joerg T. Albert

joerg.albert@ucl.ac.uk

Highlights

De novo NompC synthesis restores auditory transduction in congenitally deafened flies.

Complete turnover of NompC mechanotransducers within less than 24 hr.

Activity-dependent transcriptional control of transducers controls auditory function.

Boyd-Gibbins et al., iScience
24, 102486
May 21, 2021 © 2021 The Authors.
<https://doi.org/10.1016/j.isci.2021.102486>

Article

Turnover and activity-dependent transcriptional control of NompC in the *Drosophila* ear

Nicholas Boyd-Gibbins,^{1,5,7} Camille H. Tardieu,^{1,7} Modesta Blunskyte,¹ Nerissa Kirkwood,^{1,6} Jason Somers,^{1,2} and Joerg T. Albert^{1,2,3,4,8,*}

SUMMARY

Across their lives, biological sensors maintain near-constant functional outputs despite countless exogenous and endogenous perturbations. This sensory homeostasis is the product of multiple dynamic equilibria, the breakdown of which contributes to age-related decline. The mechanisms of homeostatic maintenance, however, are still poorly understood. The ears of vertebrates and insects are characterized by exquisite sensitivities but also by marked functional vulnerabilities. Being under the permanent load of thermal and acoustic noise, auditory transducer channels exemplify the homeostatic challenge. We show that (1) NompC-dependent mechanotransducers in the ear of the fruit fly *Drosophila melanogaster* undergo continual replacement with estimated turnover times of 9.1 hr; (2) a *de novo* synthesis of NompC can restore transducer function in the adult ears of congenitally hearing-impaired flies; (3) key components of the auditory transduction chain, including NompC, are under activity-dependent transcriptional control, likely forming a transducer-operated mechanosensory gain control system that extends beyond hearing organs.

INTRODUCTION

Ever since the seminal work of Rudolf Schoenheimer (Schoenheimer, 1946), the predominant theory of life is based on the concept of dynamic equilibria, where seemingly invariable states—or performances—are in truth the product of a homeostatic balance between assembling and disassembling processes. Questions around the molecular and mechanistic logic of homeostasis have remained at the forefront of the life sciences; their answers will also be of relevance for understanding the process of aging.

During their development and life courses, biological tissues are being constantly modeled and re-modeled. Here, the particular roles of mechanical forces in shaping developmental (Eder et al., 2017; Petridou et al., 2017) or homeostatic processes—such as adaptive bone remodeling (Rubin et al., 2006)—are becoming increasingly recognized. Examples of intra- or intercellular mechanical feedback systems include interactions with the actin cytoskeleton (Blanchoin et al., 2014) or integrin-mediated mechanotransduction (Sun et al., 2016).

The transduction of mechanical forces into biochemical signals is thus a key requirement for the development and homeostatic maintenance of all complex organs. Those organs that are themselves specialized for the transduction of minute mechanical forces, such as hearing organs, are arguably among the most complex sensory organs that have evolved (Albert and Kozlov, 2016). The act of hearing starts with the activation of auditory transducer complexes (ATCs). ATCs are formed by membrane-bound, and force-gated, mechanotransducer channels (METs), which are linked to cytoskeletal structures and interact with various motor proteins that provide adaptation and amplification (Qiu and Müller, 2018). Auditory METs (aMETs) respond to nanometer displacements of their receiver structures (such as stereociliary hair bundles in vertebrate hair cells or antennal sound receivers in Dipteran insects (Albert and Kozlov, 2016)); but, despite the documented presence of proteostasis network (PN) components (Bokolia and Mishra, 2015) required for MET localization (Lee et al., 2008; Park et al., 2013, 2015) and the knowledge that larger (Dice et al., 1979) or mechanically loaded (Kjaer et al., 2006) proteins tend to have higher turnover rates, the protein dynamics (and proteostasis) of aMETs is almost entirely unknown. The study of auditory transducer proteostasis is of scientific importance for two reasons: aMETs are (1) the most sensitive type of mechanotransducers, which are, even in the absence of audible sound, constantly flickering between open and closed

¹Ear Institute, University College London, 332 Gray's Inn Road, London WC1X 8EE, UK

²The Francis Crick Institute, 1 Midland Road, London NW1 1AT, UK

³Centre for Mathematics and Physics in the Life Sciences and Experimental Biology (CoMPLEX), University College London, Gower Street, London WC1E 6BT, UK

⁴Department of Cell and Developmental Biology, University College London, Gower Street, London WC1E 6DE, UK

⁵Present address: Stem Cells 21, 28/8 Soi Ruamrudee, Lumpini, Pathumwan, Bangkok 10330, Thailand

⁶Present address: School of Biosciences, University of Kent, Canterbury, Kent CT2 7NJ, UK

⁷These authors contributed equally

⁸Lead contact

*Correspondence:

joerg.albert@ucl.ac.uk

<https://doi.org/10.1016/j.isci.2021.102486>



states, merely responding to the gating forces provided by thermal noise (Hudspeth et al., 2000); (2) they are part of a sensory system that shows substantial age- and noise-dependent vulnerability in both humans (Liberman, 2017; Gates and Mills, 2005) and *Drosophila* (Christie et al., 2013; Keder et al., 2020). In fact, proteostasis has been recognized as a major factor in aging processes (Taylor and Dillin, 2011; Toyama and Hetzer, 2013). Advancing our knowledge of auditory transducer homeostasis thus has also the potential to guide the way to novel protective interventions in humans.

Previous studies have found that membrane proteins show higher turnover rates than synaptic or mitochondrial ones (Dörbaum et al., 2018) and some key molecular players for membrane protein turnover, such as ubiquitin, have been identified (MacGurn et al., 2012).

Protein dynamics of both cilia (the cellular sites of mechanotransduction in insect auditory neurons) (Mirvis et al., 2018; Hsu et al., 2017) and ‘stereocilia’ (the cellular sites of mechanotransduction in vertebrate auditory hair cells) (Zhang et al., 2012; Grati et al., 2006) have been studied and it has been suggested that ion channels are characterized by particularly high turnover rates; but very little is known about MET channel turnover. This is largely due to the fact that the molecular identification of aMETs has proven a scientific challenge (Qiu and Müller, 2018). At present, candidate transducer channels have been identified for both mammals (Qiu and Müller, 2018) and insects (Albert and Göpfert, 2015). In *Drosophila*, it was shown that the transient receptor potential (TRP) channel NompC (=TRPN1) is (1) essential for sound receptor function (Effertz et al., 2011), (2) required for the mechanical integrity (gating springs) of auditory transducers (Effertz et al., 2012; Zhang et al., 2015), and (3) can form a *bona fide* mechanotransducer itself (Yan et al., 2013). NompC thus meets the key criteria for being a *Drosophila* auditory transducer channel. Another essential component of fly hearing is the heterodimeric channel formed by Nanchung (Nan) and Inactive (lav), which is unique to chordotonal organs (ChOs) (Kavlie and Albert, 2013). The Nan/lav channel is required for the generation of sound-evoked compound action potential (CAP) responses from the *Drosophila* ear. The current model of *Drosophila* hearing regards NompC as the auditory transducer channel proper, with Nan/lav acting as a downstream amplifier, or modifier, channel (Albert and Göpfert, 2015).

We used NompC to study protein dynamics and transcriptional control of auditory transducers in Johnston’s organ, a large chordotonal organ (Kavlie and Albert, 2013), which forms the *Drosophila* antennal ear. Our results show that NompC-dependent transducers undergo a continual turnover with an estimated turnover time (~76% completion) of <10 hr. The *de novo* synthesis of NompC can restore auditory transducer function in congenitally hearing-impaired flies and an activity-dependent transcriptional control of NompC expression acts to re-balance important system properties (e.g., the nonlinearity, frequency selectivity, and amplification of the antennal sound receiver). Transducer turnover and dynamics are likely to form a key mechanism of *Drosophila* auditory homeostasis.

The *Drosophila* auditory system forms a powerful model to study and quantify the general act of hearing (Albert and Kozlov, 2016; Albert et al., 2020), and specifically the elementary process of auditory transduction (Albert et al., 2007a). As a direct result of a mechanical gating, force transmission between the fly’s auditory transducer channels and their external sound receiver is inherently reciprocal. Transducer gating thus introduces characteristic mechanical signatures, e.g., gating compliances (Albert et al., 2007b; Howard and Hudspeth, 1988), into the receiver’s mechanics. These circumstances allow for assessing auditory transducer function (or malfunction) in the intact ears of live flies. Partly as a result of their unique mechanical coupling to extra- and intracellular components (which hampers the heterologous analysis of candidate channel proteins), the molecular identification of auditory transducers has proven challenging (Corey, 2006; Fettiplace, 2016; Albert and Göpfert, 2015). At the time of writing, only few molecular candidates, which meet the key criteria for pore-forming subunits of true auditory transducer channels have emerged in both insects and vertebrates; these are the two transmembrane channel-like (TMC) proteins TMC1 and TMC2 in vertebrates and the transient receptor potential (TRP) channel NompC (=TRPN1) in insects. We here concentrate on the insect channel NompC. The ears of NompC-deficient (*nompC^{null}*) flies have been reported to lose the electrical responses to sound (Effertz et al., 2011), as well as the receiver’s characteristic nonlinear compliances (=stiffness drops) associated with the gating of sensitive auditory transducer channels (see ref(Effertz et al., 2012)).

RESULTS

An adult-specific rescue of congenital deafness

We were first interested to see if NompC-supplied to congenitally NompC-deficient (*nompC³*) flies upon adulthood (i.e., upon the flies’ eclosion from their pupae)—could restore auditory transducer function. To

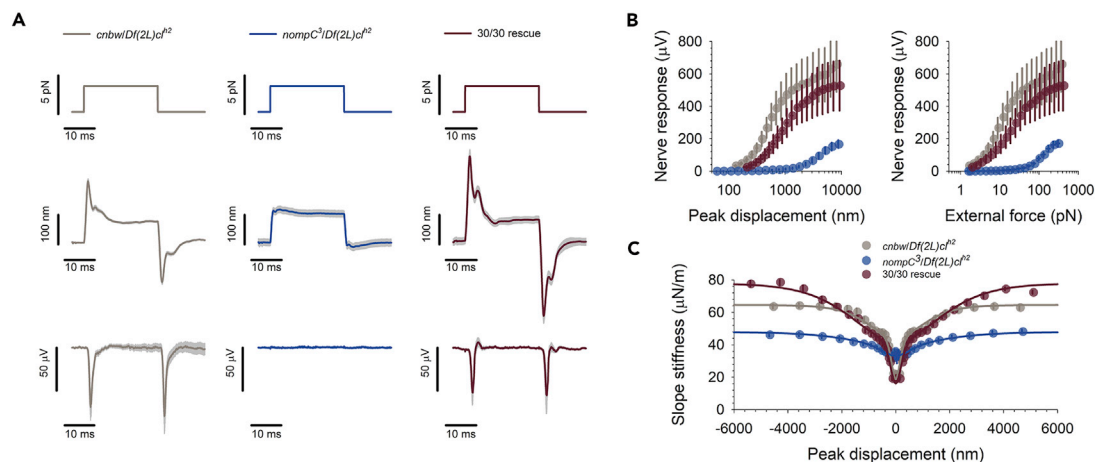


Figure 1. NompC-L-GFP fusion protein restores auditory transduction to *nompC*^{null} mutant background

(A) Mechanical and electrical responses to force step actuation of the *Drosophila* antennal ear in *cnbw* control flies (left, grey, N = 6), *nompC*³ mutants (middle, blue, N = 5) and 30/30 rescue flies (right, brown, N = 7); top traces: force steps, middle traces: antennal displacement, bottom traces: compound action potential (CAP) responses. Shaded areas show standard errors of the median.

(B) Magnitude of CAP responses as a function of antennal peak displacement (left) and size of the force step (right).

(C) Slope stiffness of the antennal receiver as a function of peak displacement. Lines show fits of a two transducer-type gating spring model. Error bars are standard errors of the median.

this end, we generated a fly line that carried (1) a *NompC*-Gal4 driver, (2) a temperature dependent suppressor of Gal4 activity (*tub-Gal80^{TS}*) together with (3) a UAS-*NompC*-L-GFP rescue construct in a *nompC*³ mutant background (henceforth simply referred to as *experimental flies*; see [Method](#) section for complete genotypes). In experimental flies, *NompC* expression would be suppressed at an ambient temperature of 18°C but expression would be initiated once flies are transferred to 30°C, thus allowing for probing an adult-onset supply of *NompC* in a *NompC*-deficient background. As a first positive control, and to test the functionality of the *NompC*-L-GFP rescue construct, we compared *nompC*^{null} flies to their *cnbw* control strain and to experimental flies that were raised and kept at 30°C (30/30 rescue) ([Figure 1](#)). We expected the 30/30 rescues to have uninhibited, control-like *NompC* supply. Consistent with previous findings ([Effertz et al., 2012](#)), the ears of our *nompC*^{null} fly strain lose the characteristic displacement overshoot ([Figure 1A](#), middle), nerve responses ([Figure 1B](#)), and gating compliances ([Figure 1C](#), blue) seen after force step actuation. The ears of 30/30 rescues, however, display all mechanical and electrical signatures of auditory transducer gating and closely resemble those of *cnbw* control flies ([Figures 1A–1C](#)). The *NompC*-L-GFP fusion protein employed in this study thus forms a fully functional transducer channel.

We then wanted to know if *de novo* synthesized *NompC* - supplied post-developmentally after the flies' eclosion from their pupae - could still be incorporated into the functional transducer complexes. This would indicate the existence of dedicated transport machinery, a crucial prerequisite for a potential homeostatic regulation of active transducer channel numbers in the adult fly ear. We compared the ears of experimental flies under two rearing conditions: (1) Flies that were raised and kept at 18°C, in which *NompC* expression should be continually blocked (18/18 continued block) and (2) flies that were raised at 18°C but moved to 30°C upon eclosion, which should block the expression of *NompC* during JO development but initiate its *de novo* synthesis in adults (18/30 adult release flies).

Comparing the two conditions reveals significant increases in all parameters of auditory transducer function in 18/30 adult release flies ([Figure 2](#)): (1) Their initial displacement overshoot after force step actuation is enhanced ([Figure 2A](#)), (2) their nerve responses are larger ([Figure 2A](#), bottom; [Figure 2B](#)), and (3) their nonlinear gating compliances are more pronounced ([Figure 2C](#)). A detailed quantitative analysis ([Figure 2D](#)) shows that the changes also include a rise in the number of predicted transducer channels. Both sensitive transducers, N_s ($p < 0.01$; ttest), and insensitive transducers, N_i ($p < 0.05$; ttest), increase significantly in 18/30 adult flies. Whereas the drop observed in single channel gating forces failed to reach significance for the sensitive transducers, z_s ($p = 0.16$; ttest), it was significantly reduced in the insensitive transducer population, z_i ($p < 0.01$; ttest). Also other key parameters of transducer mechanics, such as the asymptotic stiffness, K_{inf} ($p < 0.01$; ttest), the receiver's steady-state stiffness, K_{steady} ($p < 0.05$; ttest), the total

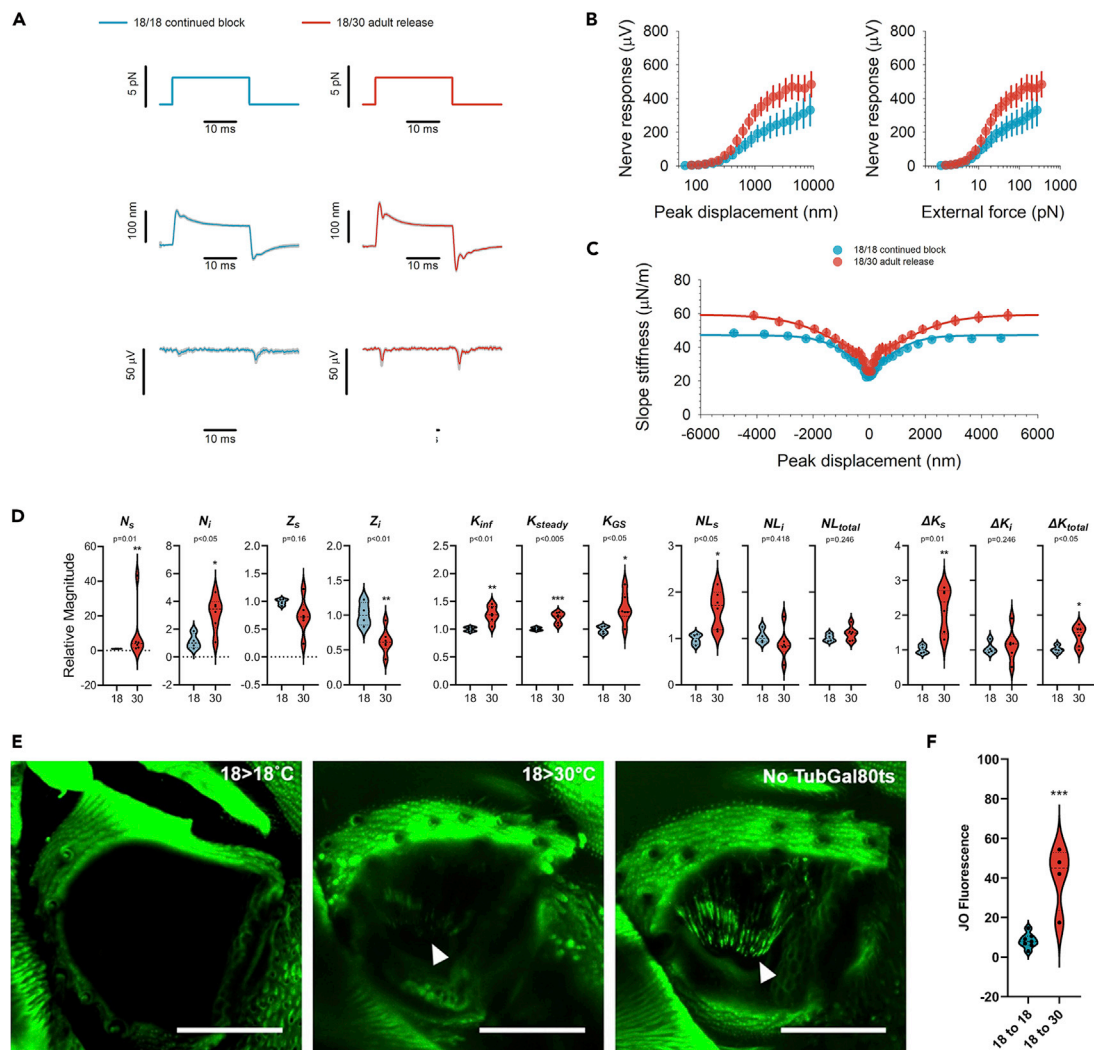


Figure 2. Adult-specific expression of NompC-L-GFP fusion protein restores key parameters of auditory transducer function to *nompC*-deficient flies (A) Mechanical and electrical responses to force step actuation of the *Drosophila* antennal ear in flies raised and kept at 18°C (18/18 continued block) (left, gray, N = 5) and flies raised at 18°C and transferred to 30°C upon eclosion (18/30 adult release) (right, brown, N = 7); top traces: force steps, middle traces: antennal displacement, bottom traces: compound action potential (CAP) responses. Shaded areas show standard errors of the median. (B) Magnitude of CAP responses as a function of antennal peak displacement (left) and size of the force step (right). (C) Slope stiffness of the antennal receiver as a function of peak displacement. Lines show fits of a two transducer-type gating spring model. Error bars are standard errors of the median. (D) Key parameters of auditory transducer function as resulting from the fits in (C). All parameters are expressed in relative terms (divided by their respective values in the 18/18 controls). Parameters (see [methods](#) and [ref\(Effertz et al., 2012\)](#)): number of sensitive (N_s) and insensitive (N_i) transducer channels; sensitive (z_s) and insensitive (z_i) single channel gating forces; asymptotic stiffness (K_{inf}); parallel stiffness (K_{steady}); gating spring stiffness (K_{GS}); extent of nonlinearity of sensitive (NL_s) and insensitive (NL_i) transducers and both combined (NL_{total}); stiffness relief for sensitive (ΔK_s) and insensitive (ΔK_i) transducers and both combined (ΔK_{total}). (E) (right) Without a Gal80^{ts} mediated block, NompC-L-GFP fluorescence is clearly visible in JO neurons and the tips of their ciliary dendrites (arrow); (left) 18/18 flies, in which NompC-L-GFP expression is blocked, lack fluorescence in JO; (middle) after an adult specific release of the Gal80^{ts} mediated block, JO neurons of 18/30 flies show clear ciliary fluorescence (arrow). Scale bars: 50 μ m. (F) Quantitative comparison of JO fluorescence in 18/18 (N = 7) and 18/30 (N = 4) flies. [For all panels: parametric or non-parametric significance tests were selected after prior checks for normality and equal variance. All indicated significances, or non-significances, remain valid (threshold $p < 0.05$) when using non-parametric tests].

gating spring stiffness, K_{GS} ($p < 0.05$; ttest), and the extent of nonlinearity of the sensitive transducer population, NL_s ($p < 0.01$; ttest), showed significant increases. The extent of nonlinearity of insensitive transducers, NL_i ($p = 0.418$; ttest), however, and the receiver's total extent of nonlinearity, NL_{total} ($p = 0.246$;

ttest), remained constant. A parameter specific to transducer function, and independent of passive receiver mechanics, is the absolute stiffness relief, ΔK , which the gating of transducers provides to the receiver. The total ΔK (ΔK_{total} , $p < 0.05$; ttest) rose significantly, but this increase was carried exclusively by the sensitive transducers, ΔK_s ($p < 0.01$; ttest), whereas the stiffness relief for insensitive transducers remained stable, ΔK_i ($p = 0.246$; ttest). Taken together, these changes are a clear indication that novel mechanotransducers have been integrated into the ciliary transduction zones of JO neurons. The rescue seen in the 18/30 flies happened on top of a partial rescue that could already be observed in the 18/18 controls. 18/18 flies thus were, in effect, not completely deaf (NompC-null) flies but rather hard-of-hearing (NompC-impaired) flies. This is either the result of an occasionally reported 'leakiness' of the UAS rescue construct or an incomplete Gal4 suppression by Gal80^{ts} (Port et al., 2020; Hudson and Cooley, 2014), which—especially for functional systems operating with very low protein numbers, such as the *Drosophila* auditory transducer machinery—can already lead to a non-specific, partial rescue (Kavlie et al., 2010). As a complete suppression of transducer function was not required for our study, we did not explore these issues further.

But as we used a temperature-controlled gene delivery paradigm for a poikilothermic—i.e., temperature-unstable—animal, the question arises if some of the observed changes reflect a direct temperature effect on auditory transduction. Previous studies have found robust temperature compensation mechanisms in insect auditory receptors (Roemschied et al., 2014), but data on the effects on auditory transduction proper are still lacking. We therefore conducted a temperature control experiment in wild-type flies (Oregon-R). We found that a temperature increase from 18°C to 30°C had indeed significant (albeit small) effects on some transducer parameters (Figure S1). All of these, however, changed the respective transducer parameters in the opposite direction as compared to the 18/30 rescue flies: Transducer numbers (N_s and N_i), for example, showed a (non-significant) tendency to decrease at 30°C, whereas they significantly increased in the 18/30 rescue flies; the stiffness relief provided by the gating of (sensitive) auditory transducers (ΔK_s) also showed a significant decrease in 30°C wild-type control flies but significantly increased in 18/30 rescue flies. The *de novo* expression of NompC, thus, not only had to rescue the functional deficits of the genetic background but also a temperature-accelerated transducer aging. These findings further validate the observed recovery.

To probe and visualize this integration more directly, we exploited the fact that our NompC rescue construct was fused to a GFP reporter. While flies raised under a continued Gal80^{ts}-mediated block of NompC expression (18/18 continued block) showed close-to-zero levels of specific fluorescence in JO (Figure 2E, left), fluorescence was restored to the apical cilia of JO neurons in 18/30 adult release flies (white arrow head in Figure 2E, middle) and showed a significant increase in fluorescent intensity at the ciliary tips (from median 7.87 to 44.97, $p = 0.0005$; ttest) compared to 18/18 flies (Figure 2F).

NompC transducers undergo continual turnover

The suggestion that newly expressed NompC keeps being transported, and functionally integrated, into the mechanotransduction sites of JO neurons opens the possibility that an *in vivo* homeostatic maintenance machinery exists, which employs transducer channel turnover to regulate JO sensitivity. To test this idea, we once again made use of the fluorescent nature of our rescue strategy. Using fluorescence recovery after photobleaching (FRAP), we quantified the turnover of NompC in the JOs of adult flies (Figure 3). FRAP analysis indeed confirmed a continuous turnover of NompC channels. While no recovery was observed 2 hr post-bleaching, fluorescence intensities rose steadily thereafter and, at 24 hr, even exceeded pre-bleach levels. The translation-to-translocation half-life of NompC, as calculated from the fluorescence recovery in fixed antennae, was ~ 3 hr (time constant, $\tau \sim 4$ hr).

Most notably here, the projected post-recovery (*asymptotic*) fluorescence intensities were higher than their pre-bleach levels ($\sim 40\%$ higher, see Figure 3C). We were wondering if this increase in NompC expression was related to the drastically reduced, effectively eliminated, antennal mobility in agar-embedded flies. If a block of antennal motion (and thus a lack of JO stimulation) leads to an upregulation of transducer channels, then this could be reflective of an underlying activity-dependent control of NompC expression.

Activity-dependent transcriptional control of NompC

We used the quantitative polymerase chain reaction (qPCR) to test this hypothesis in three separate experiments that were designed to modulate the mechanosensory input of the fly's antennal ear. As a first proof-of-principal experiment, we tried to block the ears' mechanical input by gluing one antenna while leaving

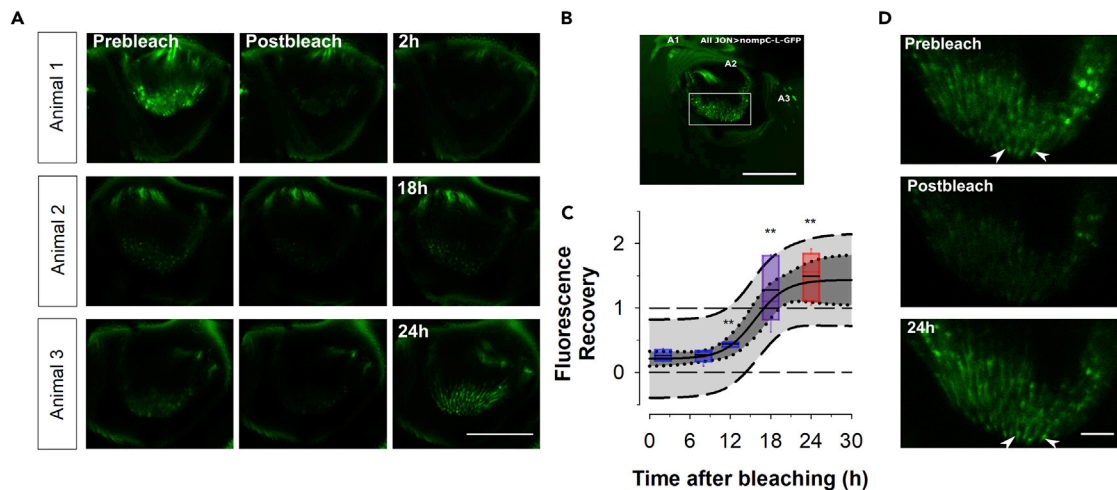


Figure 3. Fluorescent recovery after photobleaching of NompC-L-GFP

(A) Confocal images showing pre-bleach, post-bleach and post-bleach after 2 hr (top row), 18 hr (middle row) and 24 hr (bottom row). Each row shows images from an individual animal. Scale bar: 50 μ m.

(B) Z-projections of confocal images of the JO of flies expressing the rescue construct NompC-L-GFP driven by NompC-Gal4 in a null *nompC*³ background. The white box surrounds the distal cilia tips and shows the area targeted for photobleaching.

(C) Fluorescent recovery calculated from intensity values in the bleached area at different timepoints after bleaching. Boxes represent 5th and 95th percentile with the horizontal bar representing median values. Fit parameters: time constant (τ) = 2.29hr[corresponding to a \sim 76% ($=4\tau$) turnover time of 9.16hr]; initial relative fluorescence, F_{start} = 0.212; final relative fluorescence, F_{end} = 1.435; midpoint $t_{0.5}$ = 15.67hr[see Figures S3 and S4 for further details].

(D) Confocal images of the \sim 66 \times 44 μ m target areas for pre-bleach (top), post-bleach (middle) and after 24 hr (bottom). Arrowheads point to the distal cilia tips. Scale bar: 10 μ m.

the other free. After 8 hr the second antennal segments of both antennae were dissected and processed for qPCR analysis. Comparing the expression levels of *nompC* between blocked and free antennae revealed a significant ($p = 0.04996$; ttest) \sim 85% increase of expression in the blocked condition (Figure 4A). Interestingly, two other TRP channels, Nanchung (Nan) and Inactive (lav) (Gong et al., 2004; Nesterov et al., 2015)–which were previously found to be essential for mechanically evoked CAP responses from JO–also showed significant increases (\sim 122% for Nanchung($p = 0.0487$; ttest) and \sim 148% for Inactive ($p = 0.0159$; ttest) after blockage of antennal motion, suggesting activity-dependent expression control mechanisms for key mechanosensory ion channels.

However, with various neuronal populations, with differential response properties (Kamikouchi et al., 2006) and at least two types of transducer channels (sensitive and insensitive ones, ref[Effertz et al., 2012]) present in JO, the initial signaling response to our first experiment is likely to be complex. We thus chose a second approach using the (non-lethal) insecticide Pymetrozine, which specifically targets chordotonal organs (Ausborn et al., 2005). Pymetrozine’s molecular target is the heterodimeric ion channel formed by the two interdependent TRPV channels Nanchung (Nan) and Inactive (lav) (Gong et al., 2004; Nesterov et al., 2015). Functionally, Pymetrozine acts as an agonist, irreversibly opening the Nan/lav channel, rendering it insensitive to further stimulation. Previous studies showed that the initial strong Ca^{2+} response ceases after a while (Kay et al., 2016); chordotonal neurons eventually become silent and unresponsive to mechanical stimulation (Ausborn et al., 2005; Nesterov et al., 2015) or a second Pymetrozine application (Kay et al., 2016). Notably though, chordotonal neurons do not die and still remain responsive to electrical stimulation (Warren and Matheson, 2018).

Next to *nompC*, we again quantified the post-exposure expression levels of *nanchung* and *inactive*, the direct targets of Pymetrozine. For the experiments, Canton S flies were exposed to food containing 1,000 ppm Pymetrozine for 1 hr and their second antennal segments were dissected immediately afterwards, providing a first timepoint at 0 hr, followed by further timepoints at 2 hr, 4 hr, and 24 hr. The circadian state of the animal was hereby controlled, such that the time of qPCR always fell to the same circadian timepoint. All Pymetrozine exposed flies showed the reported hallmarks of proprioceptive dysfunction, mainly reflected by the incapacity to fly and a severely reduced capacity to climb. The qPCR analysis revealed a highly similar expression pattern for all three TRP channels.

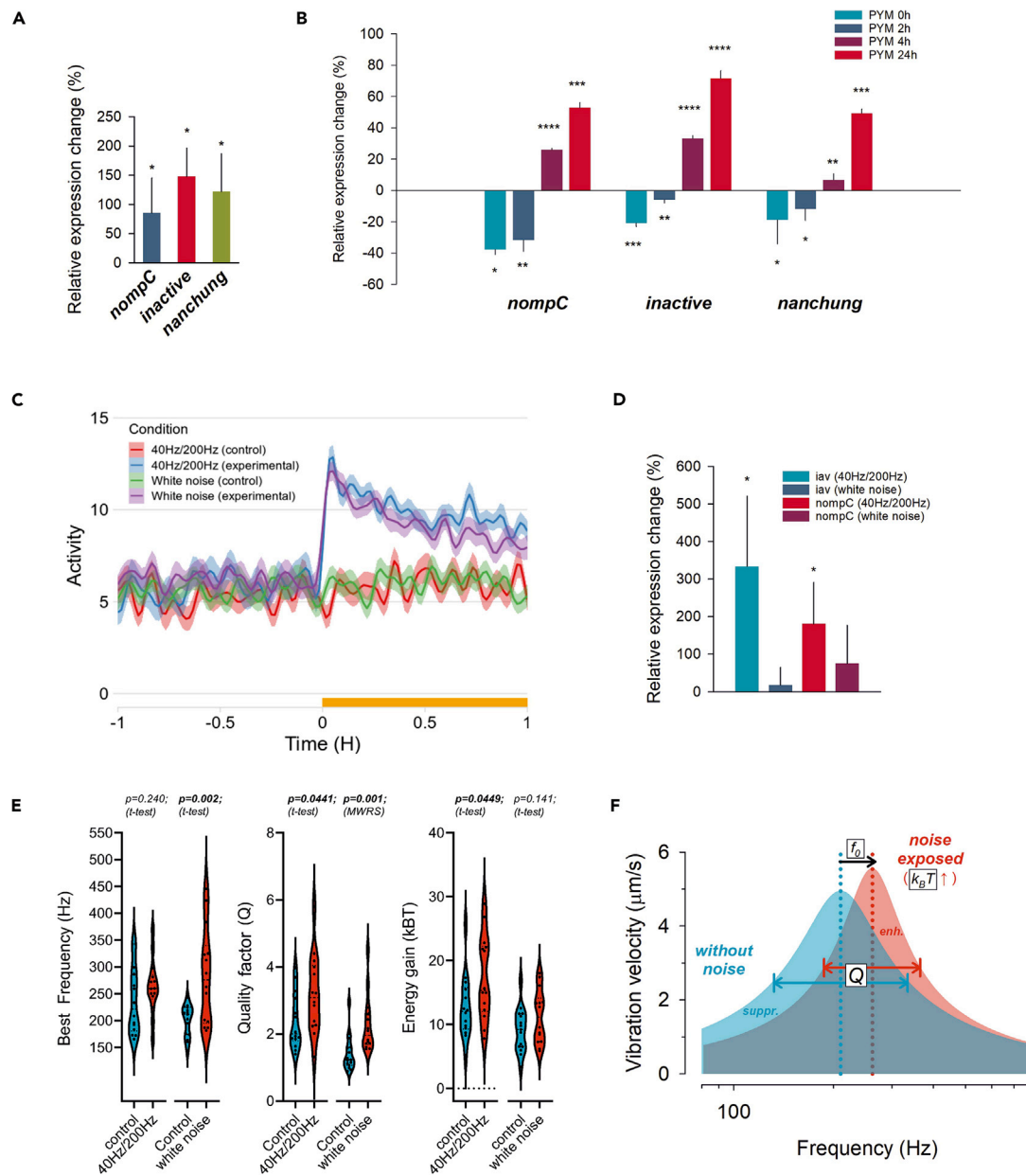


Figure 4. Activity-dependent control of *nompC* expression

(A) qPCR analysis showing relative expression of mechanotransduction genes *nompC*, *nanchung* and *inactive* in antennae blocked for 8 hr relative to their freely moving contralateral controls [three negative controls per target, three replicates for each sample and each target].

(B) qPCR analysis of mechanotransduction genes at 4 timepoints after a 1 hr-long Pymetrozine exposure: immediately after exposure (PYM 0h), 2 hr after (PYM 2h), 4 hr after (PYM 4h) and 24 hr after (PYM 24h). All qPCR relative expression levels were normalized to endogenous control (*RpL32*) Ct values and finally against control samples. Relative quantitation ($2^{-\Delta\Delta\text{Ct}}$) averages and standard deviations were calculated from technical replicates. p values are derived from t-tests of Ct values where * $p < 0.05$, ** $p < 0.01$, *** $p < 0.001$ and **** $p < 0.0001$ [three negative controls per target, three replicates for each sample and each target].

(C) Locomotor activity profiles in response to individual stimulus sequences (40/200Hz and white noise, respectively). Stimulus sequences were played in loop for 48 hr [see Figure S5 for more details].

(D) qPCR analysis of mechanotransduction genes after 48 hr long vibrational stimulation (40/200Hz and white noise). All qPCR relative expression levels were normalized to endogenous control (*RpL32*) Ct values and finally against control samples. Relative quantitation ($2^{-\Delta\Delta\text{Ct}}$) averages and standard deviations were calculated from technical replicates. p values are derived from t-tests of Ct values where * $p < 0.05$, ** $p < 0.01$, *** $p < 0.001$ and **** $p < 0.0001$ [five biological replicates and three technical replicates for each target].

Figure 4. Continued

(E) Changes of three key parameters of auditory function (left: best frequency; middle: frequency selectivity Q; right: energy gain) after 48 hr exposure to noise (40/200Hz or white noise).

(F) Schematic depiction of auditory adjustments to noise in the *Drosophila* antennal ear. Noise exposure leads to shifts in frequency tuning and increased frequency selectivity. The observed shifts, which suppress low (noise) frequencies and enhance (biologically relevant) higher frequencies, can associate with increased energy expenditure.

Immediately after exposure (timepoints 0 hr and 2 hr), the expression levels of *nompC*, *inactive*, and *nanchung* decreased, compared to their corresponding controls. At timepoint 0 hr, *nompC* expression decreased by ~38% ($p = 0.0103$; ttest) and *inactive* and *nanchung* expression by ~21% ($p = 0.0023$; ttest) and 19% ($p = 0.0196$; ttest) respectively. At timepoint 2 hr, expression levels had slightly risen but were still significantly below control values, with *nompC* expression levels decreased by ~32% ($p = 0.0023$; ttest) and *inactive* and *nanchung* levels by ~6% ($p = 0.0017$; ttest) and ~12% ($p = 0.0361$; ttest), respectively (Figure 4B). In a second phase (timepoints 4 hr and 24 hr), the expression levels were significantly higher than those of their respective controls, showing relative expression increases of ~26% (*nompC*, $p = 0.00004$; ttest), ~33% (*inactive*, $p = 0.00001$; ttest) and ~7% (*nanchung*, $p = 0.003517$; ttest) four hours post-exposure. At the 24-hr timepoint relative expression had risen further to ~53% (*nompC*, $p = 0.0001$; ttest), 72% (*inactive*, $p = 0.00002$; ttest) and 49% (*nanchung*, $p = 0.0002$; ttest), respectively.

In a third experimental series, we tested more directly how vibrational activation affects the mechanical response properties of the *Drosophila* antennal ear. To this end, we exposed flies for 48 hr to two different low-intensity vibrational regimes, which we knew to elicit behavioral responses that depend on the antennal ears. Both the combined 40/200Hz and the white noise stimulus increased the flies' locomotor activity (Figures 4C and S5). Whole animal qPCR tests revealed significant increases in *nompC* and *iav* transcript levels post-vibration in the 40/200Hz cohort but not in the white noise cohort (Figure 4D). When quantifying auditory transducer function in free-fluctuation recordings (Figure 4E), we observed a significant increase in frequency selectivity in both 40/200Hz ($p = 0.044$, ttest) and white noise cohort ($p = 0.001$, ttest) (Figure 4E, middle). This increase in tuning sharpness was accompanied by a significant increase in energy injection in the 40/200Hz ($p = 0.0449$, ttest) but not in the white noise cohort ($p = 0.141$, ttest) (Figure 4E, right). Antennal best frequencies, in turn, were significantly increased in the white noise ($p = 0.002$, ttest), but not in the 40/200Hz cohort ($p = 0.240$, ttest) (Figure 4E, left).

DISCUSSION

The fact that an adult-specific expression of NompC can rescue a functionally deficient NompC mutant background resonates with previous findings (Askew et al., 2015), which showed that transfection of mutant mouse pups with the mammalian candidate auditory channels TMC1 and TMC2 leads to a partial functional recovery of hearing in adult mice. While Askew et al. (2015) clearly demonstrated the feasibility of a transducer-channel based gene therapy, the fact that their approach succeeded also strongly suggests the existence of an underlying homeostatic machinery, which can be exploited to deliver newly synthesized transducer channels to their functional cellular sites. We here explored this question in the model system *Drosophila* using the directly gated mechanotransducer channel NompC as a 'functional probe'.

- (i) the force-transmitting, elastic chain that connects NompC to the antennal receiver will exert a permanent mechanical load on the channels, possibly leading to non-negligible molecular wear and tear;
- (ii) the extra- and intracellular tethering that is required for the gating of NompC, as well as the transducers' interaction (Nadrowski et al., 2008) with serially connected motor proteins (likely to be dyneins [Karak et al., 2015]) pose a considerable challenge for the continual replacement of functional transducer modules;
- (iii) the mechanical coupling between sound receiver and transducers means that changes in the numbers, or molecular properties, of NompC channels can be inferred *in vivo* from the antennal mechanics of intact flies. So far, NompC is the only auditory transducer channel for which this has been established.

It is thus literally the mechanics of their operation which generates both the scientific intrigue of, and the tools for, the analysis of auditory transducer homeostasis.

We here show for *Drosophila* (1) that NompC transducers transcribed *de novo* in the ears of adult flies are being translated, transported, and functionally integrated into their native sites; (2) that NompC-dependent auditory transducers undergo a continual turnover with a logistic time constant of ~ 2.3 hr (and a corresponding $\sim 76\%$ turnover time of ~ 9.1 hr), and (3) that the transcription of *nompC* is under activity-dependent control.

Ion channels have long been found to display higher turnover rates than other catalytically active proteins (Sukharev and Sachs, 2012). Reported half-lives for exchangers of mono- or divalent cations, for example, are 2–8 hr, those of cardiac gap junction proteins (e.g., Cx43) even shorter (1–3 hr) (Chen-Izu et al., 2015). Such fast turnover rates, as also found here for NompC, mean that the vast majority of channels are being replaced in the course of any given day. The dynamic regulation of membrane conductances, which takes place on transcriptional, translational, and post-translational levels, is a key feature across the entire nervous system. It has been linked to self-tuning mechanisms, which stabilize neuronal excitation thresholds around cell-specific target activity ranges for input stimuli (Marder and Prinz, 2002).

Our findings suggest a similar stabilization for the NompC-dependent neurons of JO, and possibly chordotonal organs more widely. In response to varying levels of activation, the levels of transducer genes, such as *nompC*, *nan*, or *iav* may move up or down (see Figures 4A, 4B, and 4D). The underlying activity-feedback loops appear to be part of an automatic gain control system, which recalibrates JO sensitivity to stabilize, or rebalance, the sensory output (and thus the mean *input* to downstream circuits). Our preliminary findings also indicate a spectral complexity of this process, with different forms of sensory activation leading to different transcriptional and functional responses. These responses partly appear to expend metabolic energy to shift the spectral range of the JO's responsiveness, possibly reflecting an active noise-evasion strategy (Figure 4F). An intriguing question here will be to see what the specific spectral and intensity thresholds of this gain control system are, how they are sensed molecularly; and if—and if so how—they differ between the five frequency-specific subgroups of JO neurons. Seminal work conducted on voltage-gated sodium channels (Baines and Lin, 2018) will provide valuable molecular leads for this line of research. In particular, the roles of action potential firing and its homeostatic regulator *pumilio* (Mee et al., 2004; Muraro et al., 2008) will be worth exploring.

The short turnover times of NompC transducers, as suggested by our FRAP analyses, is also consistent with the rapid transcriptional response we observed after pharmacological manipulation of TRPV-mediated currents in JO neurons. Already at time 0 hr, i.e., maximally one hour after Pymetrozine exposure, a clear down-regulation of *nompC* transcription was observed (Figure 4B). The molecular dynamics of the auditory transducer channel NompC, as well as those of the co-expressed channels *Nan* and *iav*, are remarkable, even within the established context of neuronal conductance control. In contrast to many other membrane channels, the loss of which can (at least partly) be compensated by other ion channels (O'Leary, 2018), there appears to be no degeneracy in the auditory transduction chain. A loss of NompC leads to a loss of sensitive transducer gating (Effertz et al., 2012) and sound sensitivity (Effertz et al., 2011); a loss of either *Nan* or *iav* leads to a complete loss of mechanically-evoked conductances in JO neurons (Gong et al., 2004). Any change in the density of these auditory TRP channels is thus likely to affect auditory performance, which would suggest a tight regulation. Together with previous molecular inventories of *Drosophila* hearing (Senthilan et al., 2012) and auditory homeostasis (Keder et al., 2020) these settings form an ideal, low-redundancy model of sensory homeostasis.

NompC has been shown to be part of the primary mechanotransduction pathway in JO (Effertz et al., 2012), i.e., it is mechanically coupled to the external receiver via a series of elastic components, which together form the 'gating spring' to which it contributes (Howard and Bechstedt, 2004; Zhang et al., 2015). Its removal and replacement can thus be expected to pose considerable challenges to the underlying homeostatic machinery. To make matters even more precarious, auditory transducer channels are thought to operate at very low copy numbers. Vertebrate inner ear hair cells are thought to have only two transducer channels per stereocilium (Maoileidigh and Ricci, 2019); with ~ 30 stereocilia for low-frequency hair cells to ~ 300 stereocilia for high-frequency hair cells (Rzadzinska et al., 2004); this corresponds to a total of 60–600 transducer channels per cell. Gating analyses of the fly's inner ear suggest ~ 100 –1,000 auditory (i.e., 'sensitive' as per ref (Effertz et al., 2012)) transducer units per JO; assuming ~ 100 neurons contributing to the sensitive transducer gating (JO population A + B [Kamikouchi et al., 2006]); this would correspond to only ~ 1 –10 transducer units per cell. Even if transducer units form multimeric complexes, as has been

suggested for many TRP channels, they will still operate at very low numbers and their continual replacement will have to be carefully balanced with the needs of functional continuity. One possibility here could be that homeostatic repair mechanisms are under circadian control and cluster around phases of inactivity. For the mammalian auditory system, a circadian pattern of homeostasis and vulnerability have been suggested (Basinou et al., 2017). Aware of these relations, we made a specific effort to rule out circadian distortions in our dataset. Future studies will have to address the role of the clock in *Drosophila* hearing.

Given the low numbers of active transducer channels, one could also argue that the strong fluorescence of NompC-L-GFP observable in JO cilia without antibody reinforcement is unlikely to result from only <10 GFP molecules but might rather reflect a storage buffer of ready-to-insert NompC transducers, analogous to the readily releasable pools of synaptic neurotransmitters (Kaeser and Regehr, 2017) or the Large Dense-Core Vesicles (LDCVs) that are thought to deliver receptors and signaling molecules to the neuronal membrane (Zhao et al., 2011). Whether such post-translational pools exist and, if so, how they are transported across the cilium and integrated with the existing transcriptional control loops will be one of the key questions of future research into transducer homeostasis. Finally, it is tempting to speculate that a breakdown of homeostasis is the proximate cause for multiple forms of age-related functional decline, such as age-related hearing loss (Gates and Mills, 2005; Keder et al., 2020). The turnover and activity-dependent transcriptional control of the *Drosophila* auditory transducer channel NompC reported here will help to address these questions.

Limitations of the study

The current study can show that (1) NompC continues to be transcribed, transported, and integrated into functional auditory transducer channels in the adult *Drosophila* ear and that this continual molecular renewal forms part of an activity-dependent readjustment of auditory sensitivity. Although providing some preliminary evidence in this regard, the study cannot show to what extent the molecular recycling also extends to other mechanosensory proteins. Although the study does show that stimuli with different spectro-temporal composition affect NompC transcription in different ways, the sensory logic and molecular pathways of this activity-dependent transcriptional control remain unknown.

RESOURCE AVAILABILITY

Lead contact

Joerg T Albert, Professor of Sensory Biology & Biophysics, Ear Institute, University College London, 332 Gray's Inn Road, London WC1X 8EE, UK (email: joerg.albert@ucl.ac.uk)

Materials availability

No materials were newly generated for this paper. Fly lines used were generated from publicly available lines (Bloomington *Drosophila* Stock Center; <https://bdsc.indiana.edu/>).

Data and code availability

The equations and computational logic used to analyse the data are fully listed in the [methods](#) section. All further data can be requested from the corresponding author.

METHODS

All methods can be found in the accompanying [transparent methods supplemental file](#).

SUPPLEMENTAL INFORMATION

Supplemental information can be found online at <https://doi.org/10.1016/j.isci.2021.102486>.

ACKNOWLEDGMENTS

We would like to thank Jonathan E Gale for valuable advice on the initial stages of the confocal analysis. This work received funding from the Biotechnology and Biological Sciences Research Council (BBSRC), UK (BB/L02084X/1 to JTA; BB/M008533/1 to JTA et al.; BBSRC 16Alert equipment award BB/R000549/1 to JTA et al.) and from the European Research Council (ERC) under the Horizon 2020 research and innovation program (Grant agreement Nos 648709 to JTA). CT was supported by a PhD studentship from Action on Hearing Loss, UK (grantS34).

AUTHOR CONTRIBUTIONS

Conceptualization, N.B-G., C.H.T., and J.T.A.; Investigation, N.B-G., C.H.T., M.B., N.K., J.S.; Writing—Original Draft, N.B-G., C.H.T., and J.T.A.; Methodology, C.H.T., J.S., and J.T.A.; Writing—Review & Editing, N.B-G., M.B., and J.T.A.; Visualization, N.B-G., C.H.T., M.B., J.S., and J.T.A.; Supervision, J.T.A., J.S.; Funding Acquisition, J.T.A.

DECLARATION OF INTERESTS

The authors declare no competing interests.

Received: May 11, 2020

Revised: February 17, 2021

Accepted: April 27, 2021

Published: May 21, 2021

REFERENCES

- Albert, J.T., and Göpfert, M.C. (2015). Hearing in *Drosophila*. *Curr. Opin. Neurobiol.* *34*, 79–85.
- Albert, J.T., Jarman, A.P., Kamikouchi, A., and Keder, A. (2020). 2.50 - *Drosophila* as a model for hearing and deafness. In *The Senses: A Comprehensive Reference*, Second Edition, B. Fritsch, ed. (Elsevier), pp. 985–1004.
- Albert, J.T., and Kozlov, A.S. (2016). Comparative aspects of hearing in vertebrates and insects with antennal ears. *Curr. Biol.* *26*, R1050–R1061.
- Albert, J.T., Nadrowski, B., and Gopfert, M.C. (2007a). *Drosophila* mechanotransduction—linking proteins and functions. *Fly (Austin)* *1*, 238–241.
- Albert, J.T., Nadrowski, B., and Göpfert, M.C. (2007b). Mechanical signatures of transducer gating in the *Drosophila* ear. *Curr. Biol.* *17*, 1000–1006.
- Askew, C., Rochat, C., Pan, B.F., Asai, Y., Ahmed, H., Child, E., Schneider, B.L., Aebischer, P., and Holt, J.R. (2015). Tmc gene therapy restores auditory function in deaf mice. *Sci. Transl. Med.* *7*, 295ra108.
- Ausborn, J., Wolf, H., Mader, W., and Kayser, H. (2005). The insecticide pymetrozine selectively affects chordotonal mechanoreceptors. *J. Exp. Biol.* *208*, 4451–4466.
- Baines, R.A., and Lin, W.H. (2018). Regulation of voltage-gated sodium channel expression, control of excitability and implications for seizure generation. *Curr. Opin. Physiol.* *2*, 65–70.
- Basinou, V., Park, J.S., Cederroth, C.R., and Canlon, B. (2017). Circadian regulation of auditory function. *Hear. Res.* *347*, 47–55.
- Blanchoin, L., Boujemaa-Paterski, R., Sykes, C., and Plastino, J. (2014). Actin dynamics, architecture, and mechanics in cell motility. *Physiol. Rev.* *94*, 235–263.
- Bokolia, N.P., and Mishra, M. (2015). Hearing molecules, mechanism and transportation: modeled in *Drosophila melanogaster*. *Dev. Neurobiol.* *75*, 109–130.
- Chen-Izu, Y., Shaw, R.M., Pitt, G.S., Yarov-Yarovsky, V., Sack, J.T., Abriel, H., Aldrich, R.W., Belardinelli, L., Cannell, M.B., Catterall, W.A., et al. (2015). Na⁺ channel function, regulation, structure, trafficking and sequestration. *J. Physiol.* *593*, 1347–1360.
- Christie, K.W., Sivan-Loukianova, E., Smith, W.C., Aldrich, B.T., Schon, M.A., Roy, M., Lear, B.C., and Eberl, D.F. (2013). Physiological, anatomical, and behavioral changes after acoustic trauma in *Drosophila melanogaster*. *Proc. Natl. Acad. Sci. U S A* *110*, 15449–15454.
- Corey, D.P. (2006). What is the hair cell transduction channel? *J. Physiol.* *576*, 23–28.
- Dice, J.F., Hess, E.J., and Goldberg, A.L. (1979). Studies on the relationship between the degradative rates of proteins *in vivo* and their isoelectric points. *Biochem. J.* *178*, 305–312.
- Dörbaum, A.R., Kochen, L., Langer, J.D., and Schuman, E.M. (2018). Local and global influences on protein turnover in neurons and glia. *eLife* *7*, e34202.
- Eder, D., Aegerter, C., and Basler, K. (2017). Forces controlling organ growth and size. *Mech. Dev.* *144*, 53–61.
- Effertz, T., Nadrowski, B., Piepenbrock, D., Albert, J.T., and Gopfert, M.C. (2012). Direct gating and mechanical integrity of *Drosophila* auditory transducers require TRPN1. *Nat. Neurosci.* *15*, 1198–U43.
- Effertz, T., Wiek, R., and Göpfert, M.C. (2011). NompC TRP channel is essential for *Drosophila* sound receptor function. *Curr. Biol.* *21*, 592–597.
- Fettiplace, R. (2016). Is TMC1 the hair cell mechanotransducer channel? *Biophys. J.* *111*, 3–9.
- Gates, G.A., and Mills, J.H. (2005). Presbycusis. *Lancet* *366*, 1111–1120.
- Gong, Z., Son, W., Doo Chung, Y., Kim, J., Shin, D.W., McClung, C.A., Lee, Y., Lee, H.W., Chang, D.-J., Kaang, B.-K., et al. (2004). Two interdependent TRPV channel subunits, inactive and nanchung, mediate hearing in *Drosophila*. *J. Neurosci.* *24*, 9059.
- Grati, M., Schneider, M.E., Lipkow, K., Strehler, E.E., Wenthold, R.J., and Kachar, B. (2006). Rapid turnover of stereocilia membrane proteins: evidence from the trafficking and mobility of plasma membrane Ca²⁺-ATPase. *J. Neurosci.* *26*, 6386–6395.
- Howard, J., and Bechstedt, S. (2004). Hypothesis: a helix of ankyrin repeats of the NOMPC-TRP ion channel is the gating spring of mechanoreceptors. *Curr. Biol.* *14*, R224–R226.
- Howard, J., and Hudspeth, A.J. (1988). Compliance of the hair bundle associated with gating of mechano-electrical transduction channels in the Bullfrogs Sacculus hair cell. *Neuron* *1*, 189–199.
- Hsu, K.S., Chuang, J.Z., and Sung, C.H. (2017). The Biology of ciliary dynamics. *Cold Spring Harb. Perspect. Biol.* *9*, 14.
- Hudson, A.M., and Cooley, L. (2014). Methods for studying oogenesis. *Methods* *68*, 207–217.
- Hudspeth, A.J., Choe, Y., Mehta, A.D., and Martin, P. (2000). Putting ion channels to work: mechano-electrical transduction, adaptation, and amplification by hair cells. *Proc. Natl. Acad. Sci. U S A* *97*, 11765–11772.
- Kaesler, P.S., and Regehr, W.G. (2017). The readily releasable pool of synaptic vesicles. *Curr. Opin. Neurobiol.* *43*, 63–70.
- Kamikouchi, A., Shimada, T., and Ito, K. (2006). Comprehensive classification of the auditory sensory projections in the brain of the fruit fly *Drosophila melanogaster*. *J. Comp. Neurol.* *499*, 317–356.
- Karak, S., Jacobs, J.S., Kittelmann, M., Spalthoff, C., Katana, R., Sivan-Loukianova, E., Schon, M.A., Kernan, M.J., Eberl, D.F., and Göpfert, M.C. (2015). Diverse roles of axonemal dyneins in *Drosophila* auditory neuron function and mechanical amplification in hearing. *Sci. Rep.* *5*, 17085.
- Kavlie, R.G., and Albert, J.T. (2013). Chordotonal organs. *Curr. Biol.* *23*, R334–R335.
- Kavlie, R.G., Kernan, M.J., and Eberl, D.F. (2010). Hearing in *Drosophila* requires TilB, a conserved protein associated with ciliary motility. *Genetics* *185*, 177–U291.
- Kay, A.R., Raccuglia, D., Scholte, J., Sivan-Loukianova, E., Barwacz, C.A., Armstrong, S.R., Guymon, C.A., Nitabach, M.N., and Eberl, D.F.

- (2016). Goggatomy: a method for opening small cuticular compartments in arthropods for physiological experiments. *Front. Physiol.* 7, 398.
- Keder, A., Tardieu, C., Malong, L., Fila, A., Kashkenbayeva, A., Newton, F., Georgiades, M., Gale, J.E., Lovett, M., Jarman, A.P., and Albert, J.T. (2020). Homeostatic maintenance and age-related functional decline in the *Drosophila* ear. *Sci. Rep.* 10, 7431.
- Kjaer, M., Magnusson, P., Krogsgaard, M., Moller, J.B., Olesen, J., Heinemeier, K., Hansen, M., Haraldsson, B., Koskinen, S., Esmarck, B., and Langberg, H. (2006). Extracellular matrix adaptation of tendon and skeletal muscle to exercise. *J. Anat.* 208, 445–450.
- Lee, E., Sivan-Loukianova, E., Eberl, D.F., and Kernan, M.J. (2008). An IFT-A protein is required to delimit functionally distinct zones in mechanosensory cilia. *Curr. Biol.* 18, 1899–1906.
- Liberman, M.C. (2017). Noise-induced and age-related hearing loss: new perspectives and potential therapies. *F1000Res.* 6, 927.
- MacGurn, J.A., Hsu, P.C., and Emr, S.D. (2012). Ubiquitin and membrane protein turnover: from cradle to grave. In *Annual Review of Biochemistry, Volume 81*, R.D. Kornberg, ed. (Annual Reviews), pp. 231–259.
- Maoileidigh, D.O., and Ricci, A.J. (2019). A bundle of mechanisms: inner-ear hair-cell mechanotransduction. *Trends Neurosci.* 42, 221–236.
- Marder, E., and Prinz, A.A. (2002). Modeling stability in neuron and network function: the role of activity in homeostasis. *Bioessays* 24, 1145–1154.
- Mee, C.J., Pym, E.C.G., Moffat, K.G., and Baines, R.A. (2004). Regulation of neuronal excitability through pumilio-dependent control of a sodium channel gene. *J. Neurosci.* 24, 8695–8703.
- Mirvis, M., Stearns, T., and Nelson, W.J. (2018). Cilium structure, assembly, and disassembly regulated by the cytoskeleton. *Biochem. J.* 475, 2329–2353.
- Muraro, N.I., Weston, A.J., Gerber, A.P., Luschnig, S., Moffat, K.G., and Baines, R.A. (2008). Pumilio binds para mRNA and requires nanos and brat to regulate sodium current in *Drosophila* motoneurons. *J. Neurosci.* 28, 2099–2109.
- Nadrowski, B., Albert, J.T., and Göpfert, M.C. (2008). Transducer-based force generation explains active process in *Drosophila* hearing. *Curr. Biol.* 18, 1365–1372.
- Nesterov, A., Spalthoff, C., Kandasamy, R., Katana, R., Rankl, N.B., Andrés, M., Jähde, P., Dorsch, J.A., Stam, L.F., Braun, F.-J., et al. (2015). TRP channels in insect stretch receptors as insecticide targets. *Neuron* 86, 665–671.
- O’Leary, T. (2018). Homeostasis, failure of homeostasis and degenerate ion channel regulation. *Curr. Opin. Physiol.* 2, 129–138.
- Park, J., Lee, J., Shim, J., Han, W., Lee, J., Bae, Y.C., Chung, Y.D., Kim, C.H., and Moon, S.J. (2013). dTULP, the *Drosophila melanogaster* homolog of tubby, regulates transient receptor potential channel localization in cilia. *PLoS Genet.* 9, e1003814.
- Park, J., Lee, N., Kavoussi, A., Seo, J.T., Kim, C.H., and Moon, S.J. (2015). Ciliary Phosphoinositide regulates ciliary protein trafficking in *Drosophila*. *Cell Rep.* 13, 2808–2816.
- Petridou, N.I., Spiro, Z., and Heisenberg, C.P. (2017). Multiscale force sensing in development. *Nat. Cell Biol.* 19, 581–588.
- Port, F., Strein, C., Stricker, M., Rauscher, B., Heigwer, F., Zhou, J., Beyersdorffer, C., Frei, J., Hess, A., Kern, K., et al. (2020). A large-scale resource for tissue-specific CRISPR mutagenesis in *Drosophila*. *Elife* 9, 20.
- Qiu, X.F., and Müller, U. (2018). Mechanically gated ion channels in mammalian hair cells. *Front. Cell Neurosci.* 12, 100.
- Roemischied, F.A., Eberhard, M.J.B., Schleimer, J.-H., Ronacher, B., and Schreiber, S. (2014). Cell-intrinsic mechanisms of temperature compensation in a grasshopper sensory receptor neuron. *eLife* 3, e02078.
- Rubin, J., Rubin, C., and Jacobs, C.R. (2006). Molecular pathways mediating mechanical signaling in bone. *Gene* 367, 1–16.
- Rzadzinska, A.K., Schneider, M.E., Davies, C., Riordan, G.P., and Kachar, B. (2004). An actin molecular treadmill and myosins maintain stereocilia functional architecture and self-renewal. *J. Cell Biol.* 164, 887–897.
- Schoenheimer, R. (1946). *The Dynamic State of Body Constituents* (Harvard Univ. Press).
- Senthilan, P.R., Piepenbrock, D., Ovezmyradov, G., Nadrowski, B., Bechstedt, S., Pauls, S., Winkler, M., Möbius, W., Howard, J., and Göpfert, M.C. (2012). *Drosophila* auditory organ genes and genetic hearing defects. *Cell* 150, 1042–1054.
- Sukharev, S., and Sachs, F. (2012). Molecular force transduction by ion channels - diversity and unifying principles. *J. Cell Sci.* 125, 3075–3083.
- Sun, Z.Q., Guo, S.S., and Fassler, R. (2016). Integrin-mediated mechanotransduction. *J. Cell Biol.* 215, 445–456.
- Taylor, R.C., and Dillin, A. (2011). Aging as an event of proteostasis collapse. *Cold Spring Harb. Perspect. Biol.* 3, a004440.
- Toyama, B.H., and Hetzer, M.W. (2013). OPINION Protein homeostasis: live long, won’t prosper. *Nat. Rev. Mol. Cell Biol.* 14, 55–61.
- Warren, B., and Matheson, T. (2018). The role of the mechanotransduction ion channel candidate nanchung-inactive in auditory transduction in an insect ear. *J. Neurosci.* 38, 3741–3752.
- Yan, Z., Zhang, W., He, Y., Gorczyca, D., Xiang, Y., Cheng, L.E., Meltzer, S., Jan, L.Y., and Jan, Y.N. (2013). *Drosophila* NOMPC is a mechanotransduction channel subunit for gentle-touch sensation. *Nature* 493, 221–225.
- Zhang, D.S., Piazza, V., Perrin, B.J., Rzadzinska, A.K., Poczatek, J.C., Wang, M., Prosser, H.M., Ervasti, J.M., Corey, D.P., and Lechene, C.P. (2012). Multi-isotope imaging mass spectrometry reveals slow protein turnover in hair-cell stereocilia. *Nature* 481, 520–U137.
- Zhang, W., Cheng, L.E., Kittelmann, M., Li, J., Petkovic, M., Cheng, T., Jin, P., Guo, Z., Göpfert, M.C., Jan, L.Y., and Jan, Y.N. (2015). Ankyrin repeats convey force to gate the NOMPC mechanotransduction channel. *Cell* 162, 1391–1403.
- Zhao, B., Wang, H.-B., Lu, Y.-J., Hu, J.-W., Bao, L., and Zhang, X. (2011). Transport of receptors, receptor signaling complexes and ion channels via neuropeptide-secretory vesicles. *Cell Res.* 21, 741–753.

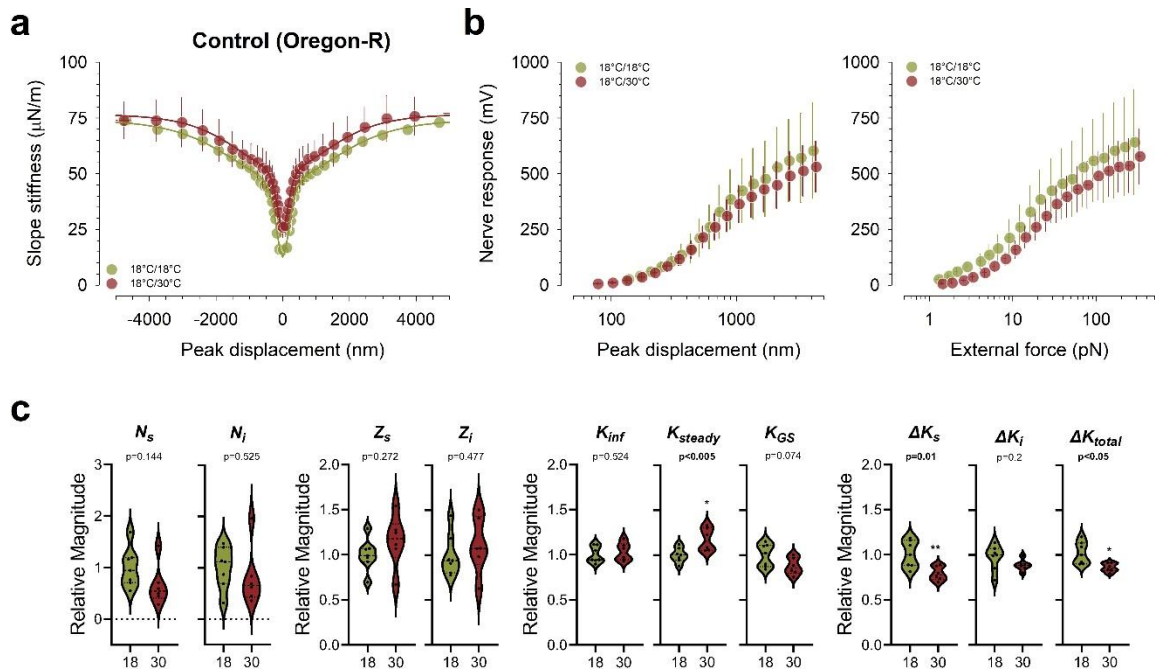
iScience, Volume 24

Supplemental information

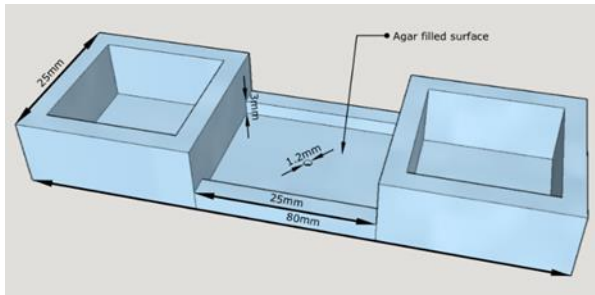
Turnover and activity-dependent transcriptional control of NompC in the *Drosophila* ear

Nicholas Boyd-Gibbins, Camille H. Tardieu, Modesta Blunskyte, Nerissa Kirkwood, Jason Somers, and Joerg T. Albert

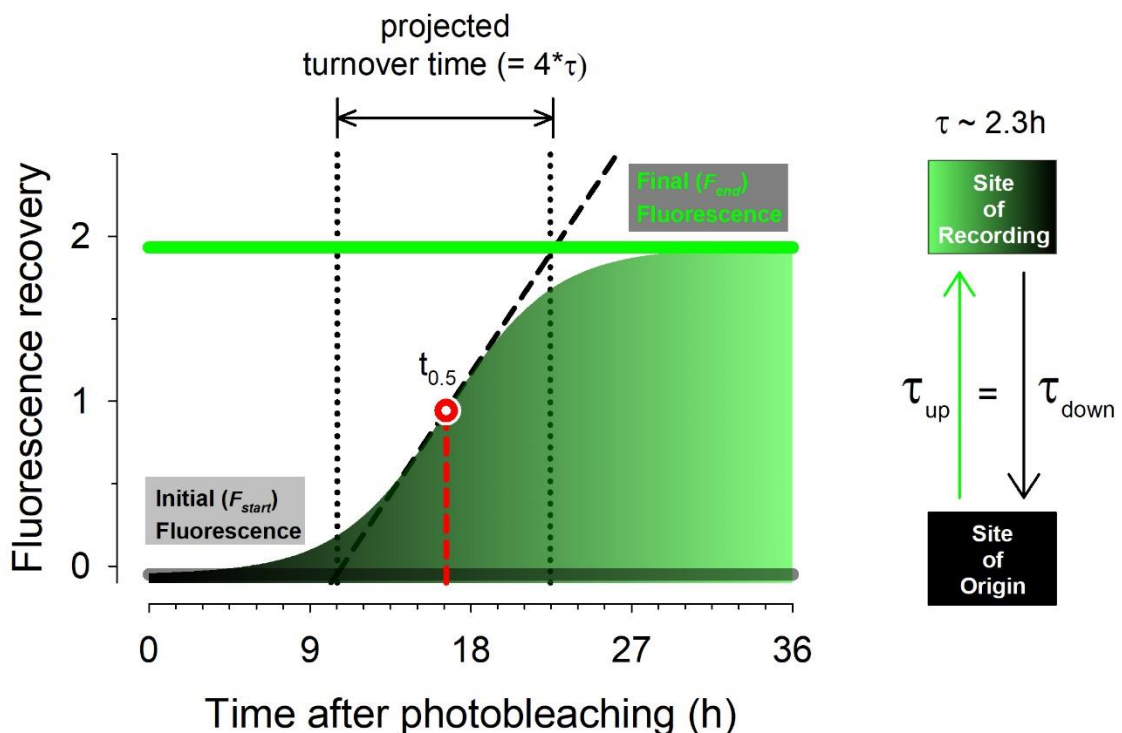
I. Supplemental Figures



Supplemental Figure 1 (related to Figure 2). Comparison of auditory transduction in [18°C /18°C] and [18°C /30°C] wildtype (Oregon-R) control flies. (a) Slope stiffness of the antennal receivers of control flies (Oregon-R) raised and kept at 18°C (18°C /18°C) (green, N=7) and flies raised at 18°C and transferred to 30°C upon eclosion (18°C /30°C) (red, N=7) as a function of peak displacement. Lines show fits of a two transducer-type gating spring model. Error bars are standard errors of the median. **(b)** Magnitude of Compound Action Potential (CAP) responses as a function of antennal peak displacement (left) and size of the force step (right) for 18°C /18°C and 18°C /30°C Oregon-R control flies. **(c)** Key parameters of auditory transducer function as resulting from the fits in (a). All parameters are expressed in relative terms (divided by their respective values in the 18°C /18°C controls). Parameters (see methods and ref. (Effertz et al., 2012)): number of sensitive (N_s) and insensitive (N_i) transducer channels; sensitive (Z_s) and insensitive (Z_i) single channel gating forces; asymptotic stiffness (K_{inf}); parallel stiffness (K_{steady}); gating spring stiffness (K_{GS}); stiffness relief for sensitive (ΔK_s) and insensitive (ΔK_i) transducers and both combined (ΔK_{total}).

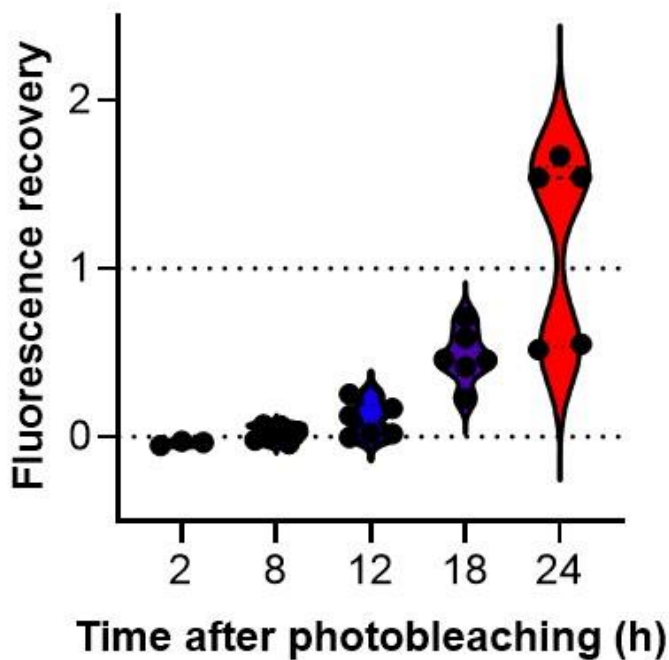


Supplemental Figure 2 (related to Figures 2 and 3). Mount for Fluorescence Recovery After Photobleaching (FRAP) experiments. The design drawings used to produce transparent acrylic fly mounts using a robotic milling machine. The two chambers at either end were used to contain ice to cool the fly and prevent movement. The central chamber was filled with agar. A 50 μ l pipette tip was inserted into the 1.2mm hole to maintain an opening while the agar set. Flies were mounted into this hole head down and fixed in position with agar cooled to around 25-30°C. Temperatures during the experiments were monitored with a ThermoProbe and kept around 25°C.

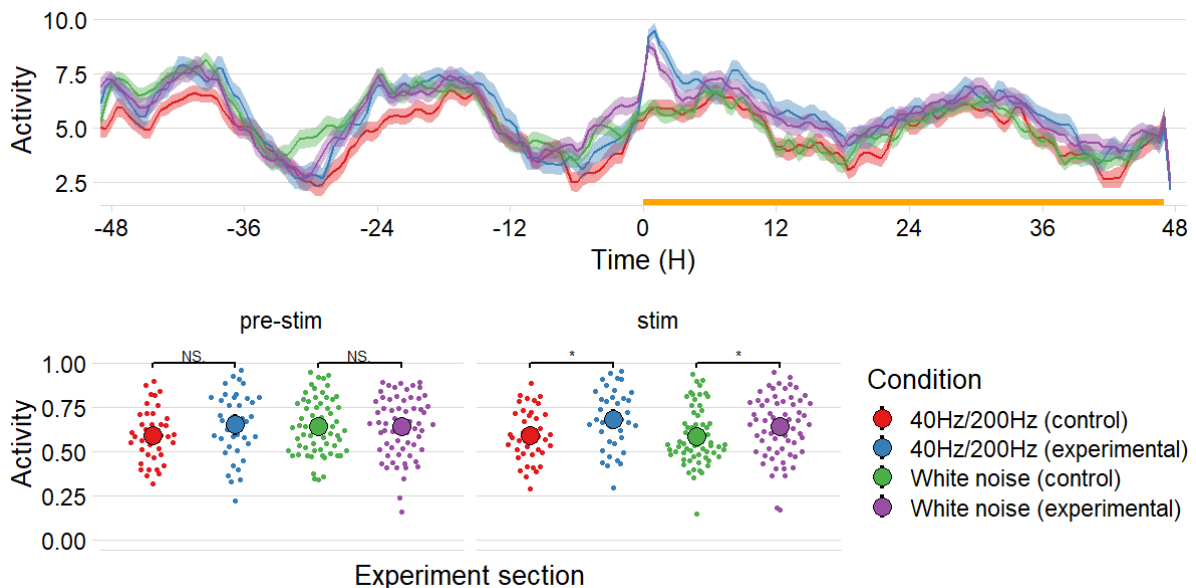


Supplemental Figure 3 (related to Figure 3). Modelling transducer turnover through Fluorescence Recovery After Photobleaching (FRAP). A sigmoidal model was fitted to the FRAP data. The inherently sigmoidal nature of the fluorescence recovery probably resulted from the fact that the effectively photobleached volume inevitably extended beyond the recording sites at the ciliary tips in which NompC is functional and the NompC-GFP signal

most concentrated. The re-emergence of fluorescent NompC thus (at least partially) required the transport (and translation) of new NompC-L-GFP proteins to the ciliary recording sites. This manifested as a time lag in the fluorescence recovery traces. Irrespective of the underlying cause of the delayed onset, however, a sigmoid function, which follows the photo recovery from an initial starting fluorescence to its final asymptotic end value, is a versatile and powerful approach to quantify the kinetics of the recovery process, and thus also the kinetics of the underlying turnover machinery. A minimal assumption model of ion channel homeostasis (and fluorescence recovery by deduction) would posit that - at dynamic equilibrium - a constant number of transducer channels signifies that the removal of old and the addition of new ion channels cancel each other out, leading to a constant fluorescence intensity (F_{end}). After photobleaching the level of fluorescence will drop to zero (if complete) or an arbitrary value below F_{end} . Depending on the noise level in the background and the extent of the bleached area (which - as stated above - might introduce transport-related delays in the fluorescence recovery trace), time lags may occur, which can be absorbed by a shift of the midpoint parameter $t_{0.5}$ (see red dotted circle and red dashed line). In all cases, the (unchanged) kinetics of the underlying turnover process will be faithfully captured within the time constant parameter (τ). The turnover time (which is calculated as $4*\tau$), finally, provides a useful estimate for the time it takes to recover the majority of bleached ion channels (corresponding to ~76% of the final, asymptotic fluorescence intensity). The here chosen definition of turnover time is the time it would take the process to move from F_{start} to F_{end} at the highest observable speed (i.e. along the line of maximum slope, see dashed line in figure). This simple equilibrium model assumes an identical time constant τ for the assembling and disassembling process (τ_{up} and τ_{down} , respectively).



Supplemental Figure 4 (related to Figure 3). Plot showing individual data points for the box plots of Figure 3c.



Supplemental Figure 5 (related to Figure 4). Plot showing locomotor activities before and during the 48h-long vibrational activation. **(top)** Average activity for each group across the experiment 48hours prior to stimulus onset to 48hours after stimulus onset (yellow bar indicates stimulus period). A one-hour low pass filter is first applied to the raw activity counts to remove high frequency noise and data is binned at 30-minute intervals. **(bottom)** Average

activity for each individual fly across the 48hours pre-stimulation (pre-stim) and of the 48hours of stimulation (stim). No significant difference between average activity is observed in the two stimulation types *prior to stimulus onset*. Significant difference between average activity is observed between both stimulation type control and experimental groups, $p = 0.011$ and $p = 0.041$ for 40/200Hz and white noise respectively, Wilcoxon Rank Sum test.

Supplemental Table 1 (related to Figure 3). Plot showing fit parameters for sigmoid recovery fits (including lower and upper confidence intervals). N=5

Parameter	Value	Lower CI (95%)	Upper CI (95%)
$t_{0.5}$ (h)	1.567e+1	1.593e+1	1.549e+1
F_{start}	2.118e-1	1.171e-1	3.033e-1
F_{end}	1.435e+0	1.101e+0	1.766e+0
τ (h)	2.287e+0	2.155e+0	2.375e+0

II. Transparent Methods

Fly lines and temperature regimes

All flies were raised on standard media at 70% humidity with a 12 hr:12 hr light:dark cycle. For temperature-controlled conditional gene expression experiments (using Gal80^{ts}) flies were kept at either 18°C or 30°C. For FRAP experiments flies were kept at 25°C. Virgin males and females were isolated on the day of eclosion using CO₂ sedation for subsequent crossing or experiments. All electrophysiological and biomechanical experiments were conducted at room temperature (18-20°C). Food was changed weekly and vials were populated with a maximum of 10 animals each.

To obtain *nompC* null mutant background fly lines with NompC rescue under temperature control the homemade balanced line carrying the second chromosome deficiency *Df(2L)c^{h2}* and the temperature-sensitive Gal4 inhibitor TubGal80^{ts} (*Df(2L)c^{h2}/Cy; tubGal80^{ts}/MKRS*) was crossed to the homemade balanced line carrying the mutant *nompC³* allele (Walker et al., 2000), a *UAS-nompC-L-GFP* construct, and the *nompC-Gal4* driver (Cheng et al., 2010) (*nompC³, UAS-nompC-L-GFP/CyO; nompC-Gal4/MKRS*).

For FRAP experiments, balanced lines were obtained by crossing homemade lines to double balancer line *y w; Sp/Cy;MKRS/TM6b* in order to create the line *nompC³, UAS-nompC-L-GFP/Cy ; NP0761/MKRS*. NP0761 flies are reported in Kamikouchi *et al.*, 2016 (Kamikouchi *et al.*, 2006) and *UAS-NompC-L-GFP* in Chen *et al.*, 2010 (Cheng *et al.*, 2010). Virgin males were collected after eclosion and aged until day 10 on normal food in a 25°C incubator submitted to 12 hour dark and 12 hour light cycles and 70% humidity. Pymetrozine experiments were conducted on 6-10 day old Canton-S males.

Biophysical and electrophysiological measurements

For analysis of JO function, flies were mounted as described previously (Albert *et al.*, 2007). Briefly, flies were attached ventrum-down to the tip of a Teflon rod using blue light cured dental glue. All potentially moving parts of the animal were secured including all legs, wing tips, and the back of the head to the upper thorax. The non-experimental (left) antenna was glued to the head to prevent any sound-induced movements or electrical signalling. The first and second antennal segments of the experimental (right) antenna were secured with glue to the head and a bridge of glue was made to the left antenna thereby anchoring the experimental antenna and ensuring all movements of the antenna were due to the experimental stimuli. The Teflon rod with the fly attached at the top was mounted in a micromanipulator that allowed accurate positioning of the fly for the experiment.

All experiments were carried out on an active vibration isolation table (model 63-564; TMC, USA). The arista of the experimental antenna was positioned perpendicular to the beam of a laser doppler vibrometer (PSV-400; Polytec, Germany) with an OFV-70 close-up unit (70 mm focal length) and a DD-500 displacement decoder. The laser beam was focused on the tip of the arista.

Two electrostatic actuators were placed in push-pull mode on either side of the arista, with one actuator ~150µm in front and one ~150µm behind the arista. A tungsten electrode (charging electrode) was inserted into the fly's thorax and used to raise the animal's electrostatic potential to ~-20V against ground. Electrostatic actuation (EA) of the antenna achieved by this setup is described in detail in refs (Albert *et al.*, 2007) and (Effertz *et al.*, 2012).

A second, electrolytically sharpened tungsten electrode (recording electrode) was inserted into the fly's head close to the base of the experimental antenna in order to make recordings of stimulus-evoked compound action potentials (CAPs) from the antennal nerve. The charging electrode also served as a reference electrode for the recording electrode.

Electrostatic force step stimulation of the antenna

At the start of each experiment, the size of the maximum command voltage (and resulting force step) was calibrated so that it produced a steady-state displacement of $\sim \pm 8\mu\text{m}$. For the force step experiments, 25ms-long step stimuli, with incrementally smaller steps, were played to the experimental antenna and the displacement responses were digitized at a rate of 100 kHz using a CED Power 1401 mk II A/D converter. Signals were loaded, and analysed, in the Spike 2 software (both Cambridge Electronic Design Ltd., Cambridge, England). The step programme consisted of 20 steps of exponentially smaller size, each step resulting in a final smallest force step of around $\sim 1\text{-}1.5$ pN magnitude. During the experiment the applied stimulus voltage and stimulus-coupled nerve responses were also recorded.

Data was analysed as described previously (Albert et al., 2007, Weinberger et al., 2017). Briefly, *Drosophila* antennae respond to force step stimuli with an initial displacement overshoot (X_{peak}) followed by a recoil after which a steady state displacement (X_{steady}) is reached. From the antennal displacement response the applied force, F , can be calculated from the maximum acceleration, \ddot{X}_{onset} , at the onset of forcing (the mass of the system is assumed to be $m = 5 \times 10^{-12} \text{g}$):

$$F = m\ddot{X}_{\text{onset}}$$

To work out the steady state stiffness (K_{steady}) the steady state displacement (X_{steady}) was found by fitting an exponential to the adaptation component of the displacement response and taking X_{steady} to equal the asymptotic value. This is then used as below:

$$K_{\text{steady}} = \frac{d(m\ddot{X}_{\text{onset}})}{dX_{\text{steady}}}$$

At the displacement peak, X_{peak} , the dynamic stiffness of the receiver can be found from:

$$K_{\text{peak}} = \frac{d(m\ddot{X}_{\text{onset}} - m\ddot{X}_{\text{peak}})}{dX_{\text{peak}}}$$

In this calculation, the effective force experienced by the receiver, $m\ddot{X}_{\text{onset}}$, takes into account the inertial forces resulting from the receiver's (non-zero) mass, $m\ddot{X}_{\text{peak}}$.

In further analyses, values for the parallel stiffness K_{par} , the gating spring stiffness, K_{GS} , and the asymptotic stiffness, K_{∞} , are determined by fitting a two transducer-type gating spring model (described below) to the force/displacement data (see (Effertz et al., 2012) for details). K_{par} is equal to K_{steady} if adaptation is complete, which has been shown for the ears of wildtype flies (Albert et al., 2007). K_{GS} , the total gating spring stiffness, is then simply calculated from $K_{\infty} - K_{steady} = K_{GS}$.

Fits of a two-transducer gating spring model

A symmetric gating spring model that includes two opposing populations of transducer complexes is fitted to the stiffness data obtained from the above described force step stimulation experiments. The gating spring model applied here is identical to the one described in (Effertz et al., 2012). Below is a summary of the model.

For each transducer channel population, the open probability is defined as:

$$p_o(X) = \frac{1}{1 + e^{-\frac{z(X-X_0)}{k_B T}}}$$

In this expression, z is the change in force in a single gating spring as the channel is opened, X_0 is the displacement of the antenna at which the open probability is 0.5, k_B is the Boltzmann constant and T is the absolute temperature. This is simplified by the assumption that $X_0 = 0$, giving:

$$p_o(X) = \frac{1}{1 + e^{-\frac{zX}{k_B T}}}$$

In the model used here it is assumed that two opposing populations of transducers have inversely related open probabilities. Hence, as the open probability of one population increases, the open probability of an opposing population decreases. As the gates of one population open, the other population's gates will close.

$$K(X) = K_{\infty} - \left(\frac{N_s z_s^2}{k_B T}\right) p_{o_s} (1 - p_{o_s}) - \left(\frac{N_i z_i^2}{k_B T}\right) p_{o_i} (1 - p_{o_i})$$

K_{∞} is here the asymptotic stiffness of the system, the stiffness of the receiver for very large displacements when all transducers are either fully open or fully closed; p_{o_s} is the open

probability of the population of sensitive transducers and p_{o_i} is the open probability of the insensitive transducers; N_s refers to the number of sensitive transducers and N_i to the number of insensitive transducers; z_s and z_i describe the respective single channel gating forces for the two transducer types.

Extent of nonlinearity

The extent of nonlinearity in the antenna's response was determined as previously described by Albert et al, 2007 (Albert et al., 2007).

As described above, the stiffness of the saturated system, K_∞ , is reduced by the contributions of two populations of transducers and depends on the single channel gating force, z , of each type of transducer, the number of channels, N , and the open probability p_0 . For open probabilities of 0.5, the stiffness relief, ΔK_s , of the system is maximum and can be written as

$$\frac{Nz^2}{4k_B T}$$

Where k_B is the Boltzmann constant (4.11×10^{-21} J) and T the absolute temperature (here 293.15 K). By dividing by the saturated stiffness, K_∞ , a ratio is obtained that describes the total extent of nonlinearity in the receiver's response, NL_{total} . This provides a ratio of the reduction in stiffness to the total stiffness of the saturated system:

$$NL_{total} = \frac{Nz^2}{(4k_B T \cdot K_\infty)}$$

This total extent of nonlinearity is comprised of both the contribution to nonlinearity of the sensitive transducers and the insensitive transducers summed together, and hence should be written as below:

$$NL_{total} = \frac{N_s z_s^2}{(4k_B T \cdot K_\infty)} + \frac{N_i z_i^2}{(4k_B T \cdot K_\infty)}$$

In this way the total extent of nonlinearity in the system can be calculated from the fit parameters obtained from fitting the gating spring model described above, and the contributions predicted made by the sensitive and insensitive populations of transducers can be also be assessed separately.

While this ratio quantifies a receiver's extent of nonlinearity, changes to its asymptotic stiffness, K_∞ , will affect this extent. Comparing the extents of nonlinearity between different flies, or different fly conditions, where K_{inf} changes, may thus be misleading.

To allow for a more direct assessment of the stiffness relief that results from auditory transducer gating, we also calculated the absolute stiffness relief, ΔK , that the two

transducer populations introduce into the receiver mechanics (as per ref. (Hudspeth et al., 2000)). For the sensitive population this stiffness relief is ΔK_s

$$= \frac{N_s z_s^2}{4k_B T}$$

and for the insensitive population this stiffness relief is ΔK_i

$$= \frac{N_i z_i^2}{4k_B T}$$

Leading to a combined stiffness relief of ΔK_{total}

$$= \frac{N_s z_s^2 + N_i z_i^2}{4k_B T}$$

FRAP mount

Agar was chosen as a suitable medium to trap flies during FRAP experiments. The use of agar allowed for minimising the amount of glue necessary to stabilise the flies in a desired position and also kept flies hydrated. An individual (one-fly) mount milled in a transparent cast acrylic plate (see Supplementary Figure 1) featuring dimensions as annotated below was used. A 1.2mm hole housed the fly, head facing down to where cover glass was attached. This mount was designed to be virtually the same size as a typical microscopic slide and suitable for an inverted microscope. It is possible to cool the mount down by inserting ice into the two wells on each side of the mount. This is particularly useful in the case of high temperatures in the confocal chamber.

The tips of 50 μ l pipettes were used to help shape an opening on the acrylic mount where the agar would be poured to set. One millilitre of 1.5% agar gel prepared with Low Gelling Temperature Agarose (Sigma-Aldrich) was cast in each mount and left to set for 30min. Some liquid agar was kept in a 37°C incubator. One hour before the experiment, the flies were mounted as follows. Flies were anaesthetised with CO₂. After 1min on CO₂, the fly was transferred into the agar opening and was carefully pushed up the small agar “tunnel” until its head was slightly above the acrylic side of the mount. At that stage, the head was rapidly fixed into position with dental glue. The glue was cured with a curing light. 20 μ l of the liquid agar preserved at 37°C and cooled down to around 25-30°C was then pipetted in the agar “tunnel”. By solidifying virtually instantly, the agar limited leg movements. Finally, a 22mm x 22mm glass coverslip with glycerol was placed on the head. The coverslip was then immobilised with electrical insulating tape.

Photobleaching and Imaging

FRAP experiments were conducted on a Zeiss LSM 510 confocal microscope. 3µm optical slice sections were acquired for pre-bleach and post-bleach stacks with a Plan-Neofluar 40x/1.3 Oil objective. The argon laser was used at 25% in order to detect GFP proteins with a 245µm pinhole. Saturated pixels were avoided by using a range indicator palette. Photobleaching was triggered and monitored manually in an area of approximately 66 x 44µm targeting the cilia previously selected from the pre-bleach stack. The argon laser power was changed to 100% at which times-series lasted an average of 300 frames for approximately 3min30sec. Once the fluorescence decay speed had reduced to minimal changes, the time-series was stopped, and the post-bleach stack was taken. For each fly, the photobleaching time, rotation of the stack and side of the antenna (right or left antenna) were logged. Between post-bleach imaging (directly after photobleaching) and recovery imaging, the mounts were kept on a plate lined with damp tissue and placed in a 25°C incubator.

Image and data analysis

The software Image J was used to quantify fluorescence intensity in pre-bleach, post-bleach and recovery stacks. On the pre-bleach stack, a rectangular region of interest (ROI) was delimited as similar as possible to the bleached area both in dimensions and in depth. The same procedure was followed for background intensities. Arrays of intensities present in the JO ROI and background ROI throughout the stack were acquired. This was repeated for post-bleach and recovery stacks. Only the fluorescence values corresponding to the bleached slice plus two slices below and two slices above were selected for analysis. These fluorescence intensity values were then calculated and analysed as follows:

$$JO_{postbleach(timepoint)} / JO_{prebleach(timepoint)}$$

Statistical tests were computed in SigmaPlot (Systat Software, Inc.): a four-parameter sigmoid fit was applied to the fluorescence recovery data points such that see also Supplemental Figure 1:

$$f = \frac{F_{start} - F_{end}}{(1 + e^{\frac{t-t_{0.5}}{\tau}})} + F_{end}$$

With t being the time of measurement, F_{start} being the relative fluorescence at $t=0$, F_{end} being the asymptotic relative fluorescence at $t=\infty$, $t_{0.5}$ being the time at 50% recovery (centre point) and τ being the time constant. Corresponding half-life values were calculated as $\tau * \ln(2)$.

Pymetrozine exposure

Pymetrozine was provided by Syngenta, UK. The powder was prepared and homogenised in MilliQ water as a 1000ppm stock (or 4.6mM). Simple sugar and agar food was prepared with 1% agar and 5% sucrose in water. 60µl of the Pymetrozine solution was applied onto the surface of the food once it had set. The solution was then left to dry overnight. Control or sham food was prepared using the same ingredients cited above without applying Pymetrozine.

Canton-S virgin males were aged 6 to 10 days. They were kept in a 12 hr:12 hr light:dark regime at 25°C. Prior to Pymetrozine exposure, the flies were starved for 1 hour in empty food vials with wet tissue to prevent desiccation. The flies were then transferred onto Pymetrozine or sham food and exposed for one hour.

Exposed flies were then transferred onto typical sugar/yeast food. Four time points were chosen: 0, 2, 4 and 24 hours after Pymetrozine exposure. In order to account for putative circadian fluctuations in mechanotransducer factors' gene expression, controls were dissected at the same four time points and at the same time of the day in a strict one-hour window. In total, 35 flies were dissected for each time point.

Dissection and RNA extraction

Flies were anaesthetised on ice and their second antennal segments were dissected in a strict one hour window. Dissection of the second antennal segment involves pulling out the third segment followed by pinching the first and second segment joint with sharp forceps in order to preserve the JO encapsulated in the second antennal segment (a2). They were then collected in 1% β-mercaptoethanol in Lysis Buffer (provided in Qiagen RNeasy Mini Kit). As soon as the dissections were completed for one time point, the samples were frozen at -25°C. After thawing on ice, samples were homogenised with an ultrasonic device (Hielscher UP200H sonicator) set at 100kHz for 20 to 30sec. The sonicator tip was carefully washed with ethanol after each use. RNA was extracted from samples according to the Qiagen RNeasy Mini Kit protocol. RNA samples were then stored at -80°C.

Reverse transcription and pre-amplification

Reverse transcription was carried out with the High Capacity RNA to cDNA kit (Applied Biosystems). RNA samples, Enzyme Mix and Buffer Mix were thawed on ice and briefly vortexed. 10µl Buffer Mix, 1µl Enzyme Mix and 9µl RNA were mixed and briefly centrifuged in

PCR tubes. Thermal cycling was programmed for 60min at 37°C and 5min at 95°C. For immediate use, cDNA was kept at 4°C.

In order to proceed to pre-amplification with TaqMan PreAmp Master Mix Kit, a “pooled assay” of Taqman primers was prepared. TaqMan primers were mixed together and diluted 1:100 in TE buffer. 25µl PreAmp Master mix, 12.5µl “pooled assay” and 12.5µl cDNA were homogenised in PCR tubes. Thermal cycling was programmed 10min at 95°C followed by 14 cycles of 15sec at 95°C and 4min at 60°C. The pre-amplified cDNA was diluted 1:20 in TE buffer and stored at 4°C if the qPCR was performed immediately after or -25°C if the qPCR was performed later.

qPCR

Real time Polymerase Chain Reactions were run on a Step One Plus ABI machine. Prior to the reaction, the 96 well plate set up was designed with the Step One Plus software. Three negative controls were run per target as well as three replicates for each sample and each target. Ribosomal Protein L32 (PRL32) was chosen as the endogenous control and day 1 sample as the control sample. Reactions were prepared in Eppendorf tubes considering the chosen reaction volume per well was 10µl containing 0.5µl TaqMan Gene Expression Assay (primer), 5µl Gene expression Assay Master Mix and 4.5µl cDNA. (See table below for list of TaqMan Gene Expression Assay). The Eppendorf tubes were centrifuged briefly and 10µl of the reaction mix was pipetted in each well in a MicroAmp Fast Optical 96-Well Reaction Plate. The plate was covered with a MicroAmp® Optical Adhesive Film and placed in the Step One Plus machine, programmed for two minutes at 50°C, ten minutes at 95°C followed by 40 cycles of 15 seconds at 95°C and one minute at 60°C.

Table 1. TaqMan Gene Expression Assay.

Gene	TaqMan probe ID	Quencher
nompC	Dm01808271_m1	FAM
inactive	Dm01833375_g1	FAM
nanchung	Dm01805137_g1	FAM
RPL32	Dm02151827_g1	VIC

Cycle threshold (C_t) values were extracted from the Step One Plus Software data analysis. The $\Delta\Delta C_t$ and relative quantitation values were calculated in Excel such that:

$$\Delta C_t = (C_t \text{ gene } x \text{ control} - C_t \text{ endogenous control})$$

$$\Delta\Delta C_t = \Delta C_t - (C_t \text{ gene } x \text{ condition} - C_t \text{ endogenous condition})$$

$$RQ = 2^{-\Delta\Delta C_t}$$

The three RQ values were averaged for each triplicate and standard deviations generated in Excel. Statistical tests were performed in Excel.

Protocols used to test activity-dependent transcriptional control and auditory tuning (48h stimulation series)

To test if vibrational stimulation affects NompC transcription levels, and functional properties of the antennal ear, flies were stimulated for 48 hours under different regimes in climate-controlled incubators (Percival Scientific, Inc., USA; 70%RH at 21°C). Individual flies were loaded into DAM5M monitors (TriKinetics Inc, USA) provided with sugar-agarose food, which were monitored on DAMSystem3 software. Activity monitors were attached to a bass loudspeaker, to allow for vibrational stimulation (equivalent to (Simoni et al., 2014)). Experiments were run with two different stimulus groups and two corresponding (silence) control groups. Stimulus patterns: (i) alternating 0.5s long 40Hz/ + 200Hz stimuli, separated by 0.5s silence and (ii) 0.5s long randomized white noise sequences (30-1,000Hz), separated by 0.5s silence. Each group comprised of 32 flies. Stimuli were designed in the Spike2 software and played through a CED Power 1401-3 A/D converter (both Cambridge Electronic Design Ltd, UK). In the 40/200Hz cohort, flies were exposed to the stimulus sequence for one minute, followed by one minute of silence. This was repeated for 48 hours until the end of experiment. Similarly, the white noise cohort were exposed to the white noise stimulus sequence for one minute followed by one minute of silence for 48h. Both stimulus cohorts had individual (silent) controls.

After 48-hour stimulation, flies were either harvested for qPCR or their auditory properties were tested in free fluctuation recordings using a Laser Doppler Vibrometer (LDV). For the free fluctuation recordings, flies were mounted as described above (see section 'Biophysical and electrophysiological measurements'). Mounted flies were left to rest for an hour to allow for recovery from the cold anaesthesia and gluing procedure.

RNA extraction from whole-body samples

A whole-body RNA harvest was performed on flies after 48 hours of exposure to the different stimulus regimes. This was used to probe for transcriptional control of mechanotransducer channels across mechanosensory organs. Flies were collected and cryopreserved in liquid nitrogen after 48-hour stimulation. Flies were homogenised in 1% β -mercaptoethanol in Lysis Buffer (provided by PureLink RNA Mini Kit) using pestle. This was followed by RNA extraction using PureLink RNA mini kit. Samples were stored at -80°C.

Reverse transcription and pre-amplification of whole-body samples

RNA samples and reverse transcription buffers were thawed on ice and briefly centrifuged (supplied by Applied Biosystems). 10X RT Buffer, 25X dNTP Mix, 10X RT Random Primers, MultiScribe Reverse Transcriptase and Nuclease-free water were briefly centrifuged. The reagents were mixed with RNA samples in PCR tubes. The thermal cycling was programmed for 10min at 25°C, 120min for 37°C, 5min for 85°C, and hold at 4°C.

The TaqMan PreAmp Master Mix Kit (provided by Applied Biosystems) was used to increase the concentration of target genes – *nompC* and *iav*. The 0.05X Pooled assay mix was prepared with TaqMan primers and nuclease-free water. Each reaction contained 25 μ l of 1X TaqMan PreAmp Master Mix, 12.5 μ l of Pooled assay mix and 12.5 μ l of cDNA. Thermal cycling was programmed as follows: 10min at 95°C, 10 cycles of 15sec at 95°C and 4min at 60°C, and the last step involved 99°C for 10min and 4°C on hold. The pre-amplified cDNA was diluted 1:100 in nuclease-free water and stored at 4°C for immediate use or at -25°C for later use.

Modification of qPCR tests for activity-dependent transcriptional control (whole body samples, 48h series)

Real Time Polymerase Chain Reactions were run on a Step One Plus ABI machine and conducted as described above. Only three modifications were made: For whole-body samples, (i) five biological replicates and three technical replicates for each target were tested; (ii) silent cohort flies were chosen as control samples; (iii) genes tested were *nompC*, *inactive* with *RpL32* as control gene (see table below).

Table 1. TaqMan Gene Expression Assay.

Gene	TaqMan Probe ID	Quencher
<i>nompC</i>	Dm01808271_m1	FAM

inactive	Dm01833375_g1	FAM
RpL32	Dm02151827_g1	VIC

References

- Albert, J. T., Nadrowski, B. & Göpfert, M. C. 2007. Mechanical signatures of transducer gating in the *Drosophila* ear. *Curr Biol*, 17, 1000-6.
- Cheng, L. E., Song, W., Looger, L. L., Jan, L. Y. & Jan, Y. N. 2010. The Role of the TRP Channel NompC in *Drosophila* Larval and Adult Locomotion. *Neuron*, 67, 373-380.
- Effertz, T., Nadrowski, B., Piepenbrock, D., Albert, J. T. & Göpfert, M. C. 2012. Direct gating and mechanical integrity of *Drosophila* auditory transducers require TRPN1. *Nature Neuroscience*, 15, 1198-U43.
- Hudspeth, A. J., Choe, Y., Mehta, A. D. & Martin, P. 2000. Putting ion channels to work: Mechanoelectrical transduction, adaptation, and amplification by hair cells. *Proceedings of the National Academy of Sciences of the United States of America*, 97, 11765-11772.
- Kamikouchi, A., Shimada, T. & Ito, K. 2006. Comprehensive classification of the auditory sensory projections in the brain of the fruit fly *Drosophila melanogaster*. *Journal of Comparative Neurology*, 499, 317-356.
- Simoni, A., Wolfgang, W., Topping, M. P., Kavlie, R. G., Stanewsky, R. & Albert, J. T. 2014. A Mechanosensory Pathway to the *Drosophila* Circadian Clock. *Science*, 343, 525-528.
- Walker, R. G., Willingham, A. T. & Zuker, C. S. 2000. A *Drosophila* mechanosensory transduction channel. *Science*, 287, 2229-34.
- Weinberger, S., Topping, M. P., Yan, J. K., Claeys, A., De Geest, N., Ozbay, D., Hassan, T., He, X. L., Albert, J. T., Hassan, B. A. & Ramaekers, A. 2017. Evolutionary changes in transcription factor coding sequence quantitatively alter sensory organ development and function. *Elife*, 6.